ARTICLE

doi:10.1038/nature14581

Glypican-1 identifies cancer exosomes and detects early pancreatic cancer

Sonia A. Melo[1]†*, Linda B. Luecke[1]*, Christoph Kahlert[1]*, Agustin F. Fernandez[2], Seth T. Gammon[3], Judith Kaye[1], Valerie S. LeBleu[1], Elizabeth A. Mittendorf[4], Juergen Weitz[5], Nuh Rahbari[5], Christoph Reissfelder[5], Christian Pilarsky[5], Mario F. Fraga[2,6], David Piwnica-Worms[3] & Raghu Kalluri[1]

Exosomes are lipid-bilayer-enclosed extracellular vesicles that contain proteins and nucleic acids. They are secreted by all cells and circulate in the blood. Specific detection and isolation of cancer-cell-derived exosomes in the circulation is currently lacking. Using mass spectrometry analyses, we identify a cell surface proteoglycan, glypican-1 (GPC1), specifically enriched on cancer-cell-derived exosomes. GPC1$^+$ circulating exosomes (crExos) were monitored and isolated using flow cytometry from the serum of patients and mice with cancer. GPC1$^+$ crExos were detected in the serum of patients with pancreatic cancer with absolute specificity and sensitivity, distinguishing healthy subjects and patients with a benign pancreatic disease from patients with early- and late-stage pancreatic cancer. Levels of GPC1$^+$ crExos correlate with tumour burden and the survival of pre- and post-surgical patients. GPC1$^+$ crExos from patients and from mice with spontaneous pancreatic tumours carry specific *KRAS* mutations, and reliably detect pancreatic intraepithelial lesions in mice despite negative signals by magnetic resonance imaging. GPC1$^+$ crExos may serve as a potential non-invasive diagnostic and screening tool to detect early stages of pancreatic cancer to facilitate possible curative surgical therapy.

Exosomes are secreted membrane enclosed vesicles (extracellular vesicles) of 50–150 nm diameter[1]. Formed during the inward budding of late endosomes, they develop into intracellular multivesicular endosomes and contain nucleic acids and proteins[2–6]. Exosomes are released into the extracellular space and enter the circulation[7–10]. The biogenesis of exosomes is not clear, therefore the term extracellular vesicles is often used[11]. Exosomes-enriched proteins include members of the tetraspanin family (CD9, CD63 and CD81), members of the endosomal sorting complexes required for transport (TSG101 and Alix) and heat-shock proteins (Hsp60, Hsp70 and Hsp90)[12]. Specific markers that distinguish cancer exosomes from normal exosomes are unknown. Identification and isolation of cancer specific exosomes in body fluids could enable the identification of DNA, RNA and proteins without contamination from non-cancer exosomes, and aid in the treatment and management of cancer.

GPC1 is a specific marker of cancer exosomes

Extracellular vesicles from cancer cells (MDA-MB-231), fibroblasts (HDF and NIH/3T3) and non-tumorigenic cells (MCF10A and E10) were isolated by ultracentrifugation[13,14], and called exosomes based on the following observations. NanoSight nanoparticle tracking analysis and transmission electron microscopy (TEM) showed extracellular vesicles of 105 ± 5 nm (mean ± s.d.) and 112 ± 4 nm in diameter, respectively[15] (Extended Data Fig. 1a, b). Immunogold TEM (IG-TEM) showed CD9 (Extended Data Fig. 1c) and flotillin1 and CD81 by immunoblot[15] (Extended Data Fig. 1d and Extended Data Table 1a). Proteins were evaluated by ultra-performance liquid chromatography–mass spectrometry (UPLC–MS)[16] (Extended Data Table 1a). Proteins from HDF, NIH/3T3, E10, MCF10A and MDA-MB-231 exosomes, included the exosomes markers TSG101, CD9 and CD63 (total number of proteins: HDF: 261, NIH/3T3: 171, E10: 232, MCF10A: 214 and MDA-MB-231: 242; Supplementary Table 1). Bioinformatic analyses revealed 48 proteins (25 cytoplasmic, 7 nuclear, 5 transmembrane, 1 membrane-anchored and 7 secreted) exclusively present in cancer exosomes (Fig. 1a, Extended Data Table 1a and Supplementary Table 1). Glypican-1 (GPC1) is a membrane-anchored protein that is overexpressed in breast and pancreatic cancer[17–19]. GPC1 was increased in breast and pancreatic cancer cell lines compared to non-tumorigenic cells (Extended Data Fig. 1e, f and Supplementary Fig. 1). Using immunoblot and IG-TEM, GPC1 was detected exclusively in cancer exosomes (Fig. 1, Extended Data Fig. 1g and Supplementary Fig. 1; HMLE cells).

We performed FACS analysis of exosomes to detect GPC1 protein (Fig. 1c). IG-TEM identified cancer exosomes with GPC1, while non-cancer exosomes did not exhibit GPC1 (Fig. 1d). Cancer exosomes from sucrose gradients or ultracentrifugation showed GPC1 (Fig. 1c, e, f, Extended Data Fig. 1h and Supplementary Fig. 1).

We implanted MDA-MB-231 cancer cells in the mammary fat pads of nude mice. The mice were bled before cancer cell inoculation, and again when tumours reached an average volume of 300, 550, 1,000 and 1,350 mm^3, and crExos were assessed for the presence of GPC1 (Extended Data Fig. 2a). The percentage of GPC1$^+$ crExos increased proportionally with tumour size and correlated with tumour burden (Extended Data Fig. 2b, c). We stably expressed green fluorescent protein (GFP)-tagged CD63 in MDA-MB-231 cells. CD63 is an established exosomal marker[14], and MDA-MB-231-CD63–GFP-derived

[1]Department of Cancer Biology, Metastasis Research Center, University of Texas MD Anderson Cancer Center, Houston, Texas 77054, USA. [2]Cancer Epigenetics Laboratory, Institute of Oncology of Asturias (IUOPA), HUCA, Universidad de Oviedo, 33006 Oviedo, Spain. [3]Department of Cancer Systems Imaging, The University of Texas M.D. Anderson Cancer Center, Houston, Texas 77054, USA. [4]Department of Surgical Oncology, The University of Texas MD Anderson Cancer Center, Houston, Texas 77030, USA. [5]Department of Gastrointestinal, Thoracic and Vascular Surgery, Medizinische Fakultät Carl Gustav Carus, Technische Universität Dresden, Fetscherstr. 74, 01307 Dresden, Germany. [6]Department of Immunology and Oncology, National Center for Biotechnology, CNB-CSIC, Cantoblanco, 28049 Madrid, Spain. †Present address: Instituto de Investigação e Inovação em Saúde, Universidade do Porto, Portugal, Institute of Pathology and Molecular Immunology of the University of Porto (IPATIMUP), 4200 Porto, Portugal.

*These authors contributed equally to this work.

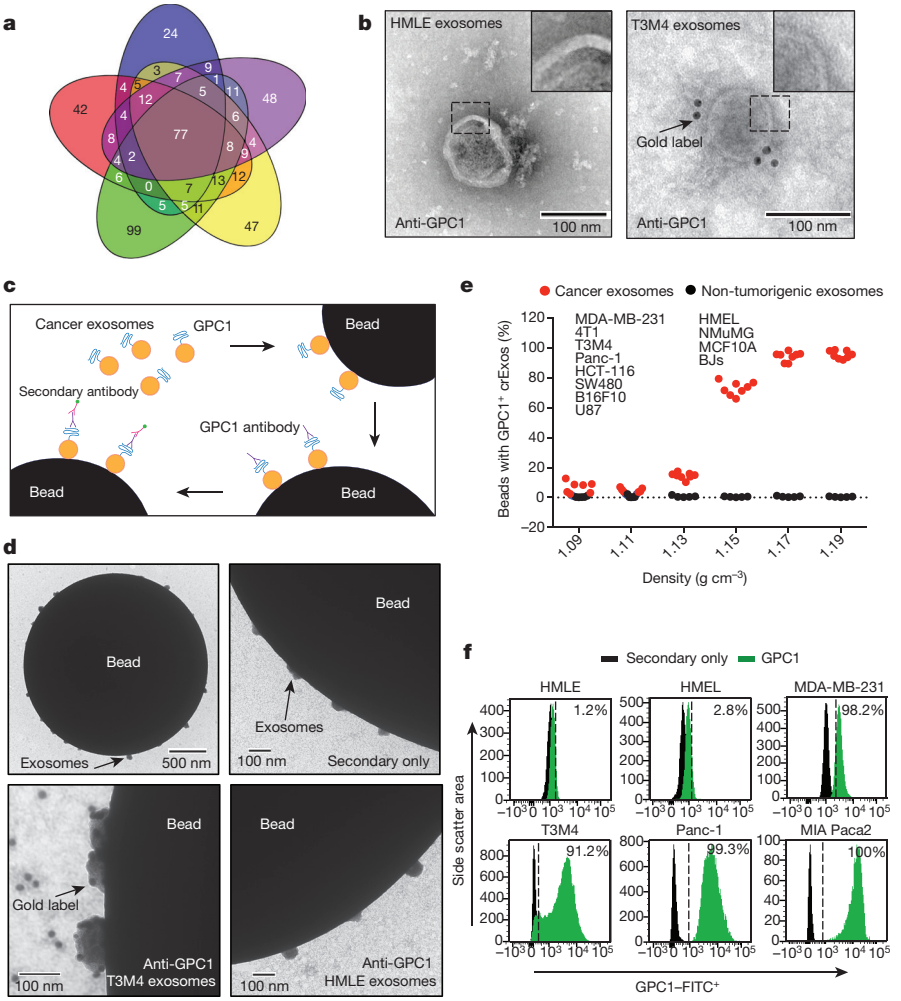

Figure 1 | GPC1 is present on cancer exosomes. **a**, Venn diagram of proteins from NIH/3T3 (blue), MCF10A (red), HDF (green), E10 (yellow) and MDA-MB-231 (purple) exosomes. In total, 48 proteins were exclusively detected in MDA-MB-231 exosomes ($n = 3$ protein samples, technical replicates). **b**, TEM (left) and IG-TEM (right) of GPC1. Top right, digitally zoomed inset ($n = 2$ experiments). **c**, Diagram of flow cytometry (FACS). **d**, TEM of bead-bound exosomes and immunogold labelling of GPC1 ($n = 2$ biological replicates). **e**, Percentage of GPC1$^+$exosome beads from cancer (red) and non-cancer cells (black). **f**, FACS of the percentage of GPC1$^+$ exosome beads ($n = 2$ biological replicates). Negative control: secondary antibody only.

exosomes were uniformly positive for GFP (Extended Data Fig. 2d). crExos were also collected from mice with orthotopic MDA-MB-231-CD63–GFP tumours, and a subpopulation of the crExos were GFP$^+$ (Extended Data Fig. 2e). GPC1 expression was exclusively detected in the GFP$^+$ crExo fraction but not in GFP$^-$ crExos (Extended Data Fig. 2f).

GPC1$^+$ circulating exosomes are a cancer biomarker

Next, we isolated crExos from patients with breast cancer ($n = 32$), pancreatic ductal adenocarcinoma (PDAC, $n = 190$) and healthy donors ($n = 100$) (patient data in Extended Data Table 2a). TEM analysis of crExos isolated from the serum revealed a lipid bilayer and CD9 positivity (Extended Data Fig. 3a, b). crExos from sucrose gradient purification also showed expression of the exosomes marker flotillin1 (Extended Data Fig. 3c, Supplementary Fig. 1)[14,15]. The relative concentration of crExos was significantly higher in the sera of cancer patients compared to healthy donors (Extended Data Fig. 3d), and the average size of PDAC crExos was significantly smaller than all other crExos (Extended Data Fig. 3e). Analyses of sera from healthy donors revealed baseline positivity for GPC1 in crExos, ranging from 0.3 to 4.7% (average of 2.3%; Fig. 2a). We observed that 75% of patients with breast cancer (24 out of 32) demonstrated GPC1$^+$ crExos levels higher than healthy donors ($P < 0.0001$; Fig. 2a). Any specific correlation between the level of GPC1$^+$crExos and breast cancer subtypes was not appreciated in this patient cohort (luminal A, luminal B or triple-negative subtypes; Extended Data Fig. 3f). By contrast, all 190 PDAC patients revealed higher levels of GPC1$^+$crExos than in healthy donors ($P < 0.0001$; Fig. 2a and Extended Data Fig. 8a, b). These results indicated a strong correlation between GPC1$^+$crExos and cancer, particularly for PDAC.

GPC1$^+$ crExos contain oncogenic *KRAS*^{G12D}

Exosomes contain DNA and RNA[20]. *KRAS* is a frequently mutated gene in pancreatic cancer and mutant transcripts have been found in circulation[3,21,22]. Primary PDAC tumour samples of 47 PDAC patients were sequenced to assess *KRAS* status. Of these, 16 contained wild-type *KRAS*, 14 contained *KRAS*^{G12D} (which encodes the KRAS glycine-to-aspartic-acid substitution mutant), 11 *KRAS*^{G12V}, 5 *KRAS*^{G12R} and 1 *KRAS*$^{G12V/C}$ mutation (Fig. 2b). Sufficient amount of corresponding serum was available from 10 patients with *KRAS*^{G12D} and 5 *KRAS*^{G12V} mutations. IG-TEM in GPC1$^+$ and GPC1$^-$ crExos from the same patient confirmed GPC1 presence (Fig. 2c). All 15 GPC1$^+$ crExos with tumour validated *KRAS* mutation revealed identical mutation by quantitative PCR of exosomal messenger RNA (Fig. 2d). Wild-type *KRAS* mRNA was found both in GPC1$^+$ and GPC1$^-$ crExos, while mutant *KRAS* transcript was only detected in the GPC1$^+$ crExos (Fig. 2d).

GPC1$^+$ crExos detect early pancreatic cancer

Analysis of the discovery cohort revealed that the levels of GPC1$^+$ crExos distinguish patients with histologically validated pancreatic cancer precursor lesions (PCPL, $n = 5$; Extended Data Table 2a) from healthy donors and patients with benign pancreatic disease (BPD, $n = 26$; Extended Data Table 2a, b and Fig. 2e). Specifically, the levels of GPC1$^+$ crExos in the PCPL group (intraductal papillary mucinous neoplasm (IPMN); $n = 5$) were consistently higher than the levels of GPC1$^+$crExos in the healthy donor group, as well as in the BPD group (which includes 18 patients with pancreatitis and 8 with cystic adenomas; Fig. 2e). All patients in PCPL group presented with specific clinical symptoms and exhibited a macroscopic mass using MRI or computed

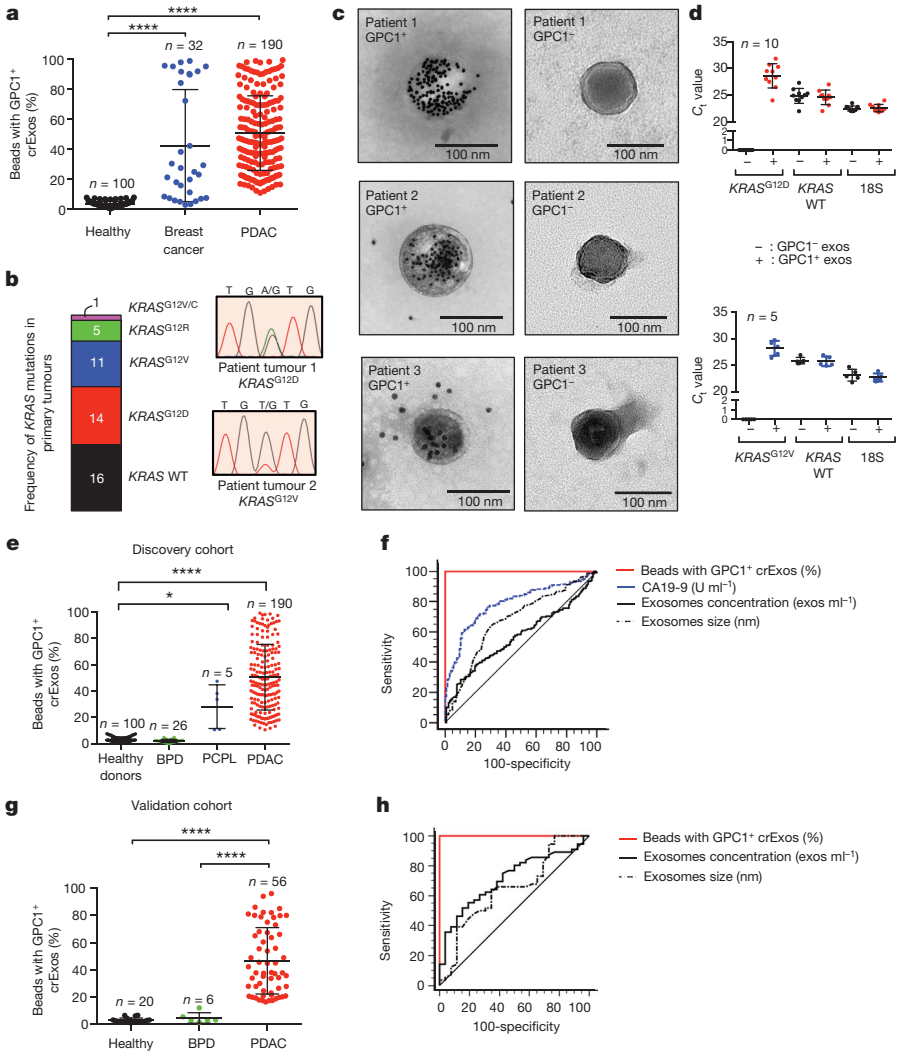

Figure 2 | GPC1$^+$ crExos are a non-invasive biomarker for pancreatic cancer. **a**, Percentage of GPC1$^+$crExo beads in healthy donors, patients with breast cancer and patients with PDAC (analysis of variance (ANOVA), post-hoc Tamhane T_2, $^{****}P < 0.0001$). **b**, Frequency of *KRAS* mutation in 47 tumours and representative DNA sequencing chromatograms. WT, wild type. **c**, IG-TEM of GPC1 of crExos from 3 PDAC patients following FACS isolation of GPC1$^+$ (left) and GPC1$^-$ (right) crExos ($n = 3$, 3 technical replicates). **d**, C_t value for $KRAS^{G12D/G12V}$, *KRAS* wild-type mRNA and 18S ribosomal RNA expression in GPC1$^+$ (red and blue) and GPC1$^-$ (black) crExos (after FACS isolation; $n = 2$, 2 biological replicates and 3 technical replicates each). **e**, Percentage of GPC1$^+$ crExo beads in the discovery cohort (ANOVA, post-hoc Tamhane T_2, $^{**}P < 0.01$, $^{****}P < 0.0001$; 3 technical replicates). **f**, ROC curve of discovery cohort. **g**, Percentage of GPC1$^+$ crExo beads in the validation cohort (ANOVA, post-hoc Tukey-Kramer test, $^{****}P < 0.0001$; 3 technical replicates). **h**, ROC curve of validation cohort. Data are mean ± s.d.

tomography. The BPD group exhibited similar GPC1$^+$ crExos levels (average 2.1% GPC1$^+$ crExos) to healthy donors (Fig. 2e).

We compared the specificity and sensitivity of GPC1$^+$ crExos to levels of carbohydrate antigen 19-9 (CA19-9; also known as sialyl Lewis^A), the clinical standard tumour biomarker for patients with PDAC[23]. CA19-9 levels were increased in the serum of patients with PDAC when compared to healthy donors, but CA19-9 levels were also significantly increased in the serum of patients with BPD ($P < 0.0001$; Extended Data Fig. 3g). Notably, CA19-9 levels failed to distinguish patients with PCPL from healthy donors (Extended Data Fig. 3g). When comparing patients with stage I–IV pancreatic cancer to healthy donors and patients with BPD, the receiver operating characteristic (ROC) curves show that GPC1$^+$ crExos revealed a near perfect classifier with an AUC of 1.0 exhibiting a sensitivity and specificity of 100%, and with a positive and negative predictive value of 100% (Fig. 2f and Extended Data Fig. 4a–f). By contrast, CA19-9 was inferior in distinguishing patients with PDAC from healthy donors ($P < 0.001$; Fig. 2f and Extended Data Fig. 4a–f). Of note, neither the concentration of exosomes nor their size was a valid parameter to distinguish PDAC patients from controls (Fig. 2f and Extended Data Fig. 4a–f). GPC1$^+$ crExos showed a sensitivity and specificity of 100% in each stage of pancreatic cancer (carcinoma *in situ*, stage I as well as stages II–IV), supporting its utility as a biomarker for all stages of pancreatic cancer and its potential for early detection of the disease.

An independent patient cohort, composed of 6 patients with histologically validated BPD (chronic pancreatitis), 56 patients with PDAC and 20 healthy donors, was used to validate our findings (Extended Data Table 2a). GPC1$^+$ crExos distinguished patients with PDAC from healthy donors and BPD patients (Fig. 2g). The BPD group exhibited similar GPC1$^+$ crExos levels to healthy donors (Fig. 2g). In complete agreement with the discovery cohort, ROC curves indicated that GPC1$^+$ crExos (from patients with PDAC or BPD and healthy donors) revealed a near perfect classifier with an AUC of 1.0, and sensitivity, specificity, positive and negative predictive values of 100% (Fig. 2h and Extended Data Fig. 4g).

GPC1$^+$ crExos inform pancreatic cancer burden

We next sought to evaluate whether GPC1$^+$ crExo levels could inform on metastatic disease burden of PDAC patients (Extended Data Table 2a). GPC1$^+$ crExos of PDAC patients with distant metastatic disease showed significantly higher levels of bead-bound GPC1$^+$ crExos (average 58.5%) than patients with metastatic disease restricted to lymph nodes (average 50.5%) or no metastases (average 39.9%; Extended Data Fig. 5a). Furthermore, we evaluated GPC1$^+$ crExos in serum of PDAC patients at pre- and post-surgery stages (post-operative day 7; PDAC $n = 29$, PCPL $n = 4$ and BPD $n = 4$; Fig. 3a). In total, 28 out of 29 PDAC patients and all PCPL patients with longitudinal blood collections showed a significant decrease in GPC1$^+$ crExo levels after surgical resection (PDAC: $P < 0.0001$; PCPL: $P < 0.001$; Fig. 3b). By contrast, CA19-9 levels decreased in only 19 out of 29 PDAC patients, and in none of the PCPL patients (PDAC: $P = 0.003$; PCPL: $P = 0.81$; Extended Data Fig. 5b). In 4 BPD patients, neither the levels of GPC1$^+$ crExos nor the levels of CA19-9 showed a difference (Fig. 3b and Extended Data Fig. 5b).

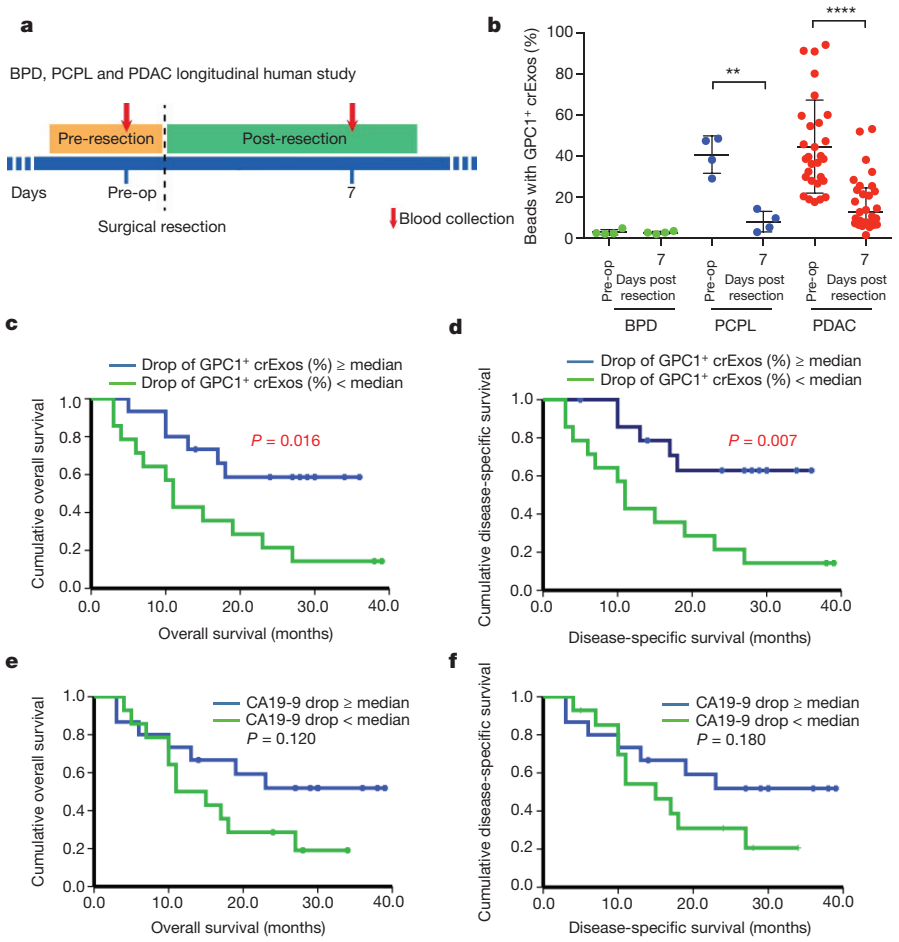

Figure 3 | Levels of circulating GPC1$^+$ exosomes inform pancreatic cancer resection outcome. **a**, Longitudinal blood collection pre- and post-operatively (day 7). **b**, Percentage of GPC1$^+$crExo beads from patients with BPD ($n = 4$), PCPL ($n = 4$) or PDAC ($n = 29$) (paired two-tailed Student's t-test, $^{**}P < 0.01$, $^{****}P < 0.0001$). Data are mean ± s.d. **c**, **d**, Kaplan–Meier curves (log-rank test) displaying overall (**c**) and disease-specific (**d**) survival of patients with a GPC1$^+$crExo drop ≥ median drop (blue), and with a GPC1$^+$ crExo drop < median drop (green) after resection. **e**, **f**, Kaplan–Meier curves (log-rank test) displaying overall (**e**) and disease-specific (**f**) survival of patients with a CA19-9 drop ≥ median (blue), and a CA19-9 drop < median (green) drop after resection.

To determine the prognostic relevance of GPC1$^+$ crExos in this longitudinal study (Fig. 3a), patients were dichotomized into two groups. Group 1 was defined by a decrease of GPC1$^+$ crExos greater or equal to the median decrease in GPC1$^+$ crExos, and group 2 was defined by a decrease of GPC1$^+$crExos that was less than the median decrease of GPC1$^+$ crExos. Group 1 presented with improved overall (26.2 months) and disease-specific (27.7 months) survival when compared to group 2 (15.5 months for both overall and disease-specific; Fig. 3c, d). Although a decrease in CA19-9 levels is noted, this decrease did not significantly associate with overall and disease-specific survival (Fig. 3e, f and Extended Data Fig. 5b). Using a Cox regression model for a multivariate analysis confirmed the decrease in GPC1$^+$crExos, as an independent prognostic and predictive marker for disease-specific survival (Extended Data Fig. 5c, d).

Next, we evaluated whether an ELISA for circulating GPC1 could function with the same specificity and sensitivity as GPC1$^+$ crExos. Serum samples of the validation cohort (20 healthy donors, 6 BPD and 56 PDAC patients) were analysed for circulating GPC1 levels. While GPC1 levels were significantly higher in patients with PDAC than in patients with BPD and healthy donors, the sensitivity and specificity of the assay was lower when compared to GPC1$^+$ crExos. The GPC1 ELISA was similar to circulating CA19-9 assay. ROC curves indicated that circulating GPC1 protein shows an AUC of 0.781 a sensitivity of 82.14%, a specificity of 75%, and positive and negative predictor values of 4% and 100%, respectively (Extended Data Fig. 5e, f).

GPC1$^+$ crExos detect early PanIN lesions

We next evaluated the longitudinal appearance in the serum of GPC1$^+$crExos relative to pancreatic tumour burden. To this end, we used a genetically engineered mouse model (GEMM) for PDAC. The *Ptf1a*$^{cre/+}$; *LSL-Kras*$^{G12D/+}$; *Tgfbr2*$^{L/L}$ (PKT) mice[24] develop PDAC with full penetrance that reliably recapitulates the clinical and histopathological features of the human disease[24,25]. The PKT mice consistently progress from pancreatic intraepithelial neoplasia (PanIN) at 4.5 weeks of age and die at 8 weeks of age owing to PDAC[24,25] (Extended Data Fig. 6a). In a longitudinal study, we bled PKT and littermate control mice repeatedly at 4, 5, 6, 7 and 8 weeks of age ($n = 7$ PKT mice and $n = 6$ control mice; Fig. 4a). Then 3 out of 7 PKT mice were euthanized by week 7, along with 4 out of 6 controls, while the remaining 3 PKT mice and 2 controls were euthanized at week 8. At 4 weeks of age, PKT mice showed on average an 8.4% elevation in GPC1$^+$ crExos, and this increased proportionally with time (and tumour burden) and severity of disease (histopathology), whereas control mice showed an average of 1.2% GPC1$^+$ crExos and this level remained constant with time (Fig. 4b). crExo sizes and concentration did not consistently correlate with disease over time (Extended Data Fig. 6b, c). MRI[26] was performed at the same time points when mice were bled to measure GPC1$^+$ crExos (Fig. 4c). When evaluated as a group, GPC1$^+$ crExo levels appeared before MRI detectable pancreatic masses (Fig. 4c, d and Extended Data Fig. 6d). GPC1$^+$ crExo size and concentration minimally correlated with pancreatic cancer (Extended Data Fig. 6b, c), whereas GPC1$^+$crExo levels correlated with tumour volume determined by MRI, and appeared to lead the growth of the tumour (Pearson correlation test, $r = 0.67$, $P = 0.0005$; Fig. 4c, d and Extended Data Fig. 6d). Notably, no increase in GPC1$^+$ crExo levels was noted in a mouse model of cerulein-induced acute pancreatitis, supporting the idea that the GPC1$^+$ crExo increase is pancreatic-cancer-specific (Extended Data Fig. 6e). The ROC curve of GPC1$^+$crExos showed an AUC of 1.0 in PKT compared to healthy littermate control mice at all ages evaluated (Fig. 4e and Extended Data Fig. 6f).

A cross-sectional study assayed tumour burden and GPC1$^+$ crExos in PKT mice, as early as 16 and 20 days of age, when they present with

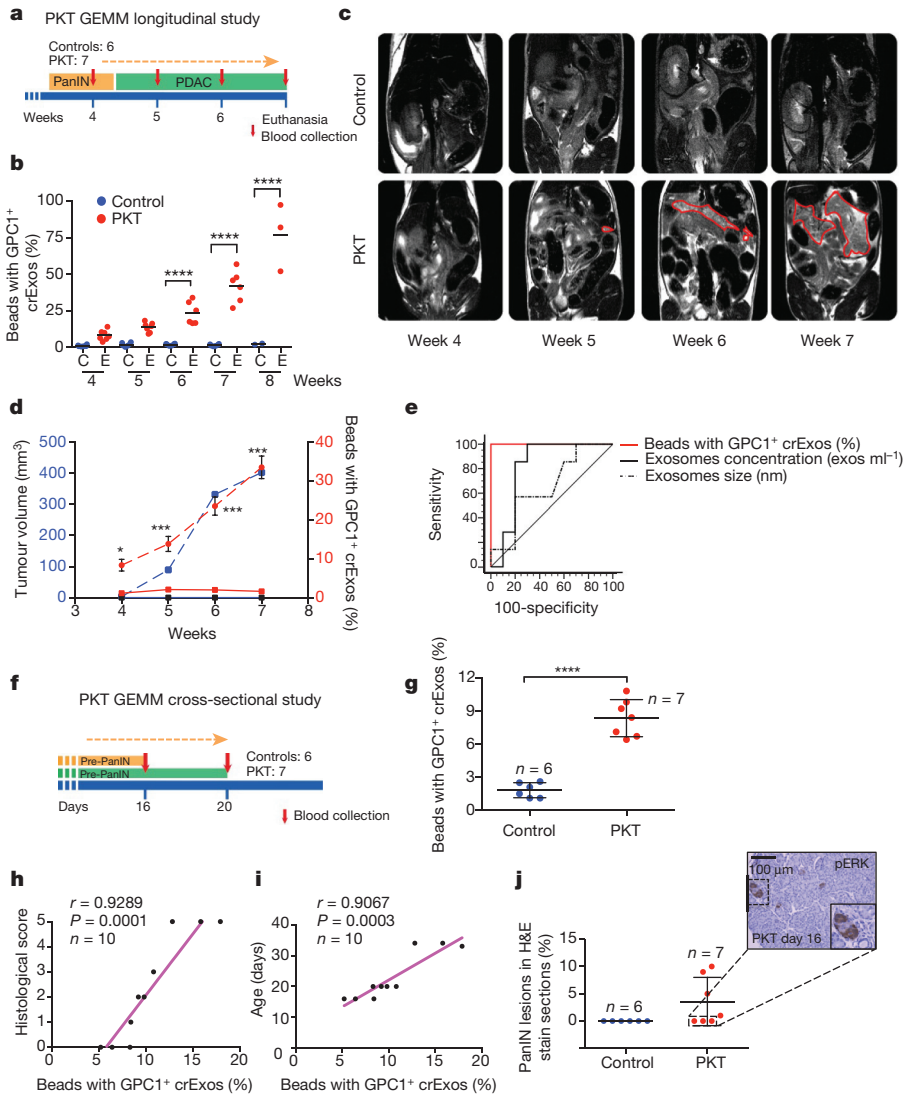

Figure 4 | GPC1$^+$ circulating exosomes predict pancreatic cancer in GEMMs. **a**, Longitudinal blood collection of control and PKT mice, at 4 ($n = 6$ and $n = 7$, respectively), 5 ($n = 6$ and $n = 7$), 6 ($n = 6$ and $n = 6$), 7 ($n = 6$ and $n = 6$) and 8 ($n = 2$ and $n = 3$) weeks of age. **b**, Percentage of GPC1$^+$ crExo beads from PKT (red) and control (blue) mice (ANOVA, post-hoc Tukey–Kramer test, $^{****}P < 0.0001$; 3 technical replicates). **c**, MRI with tumour encircled in red. **d**, Tumour volume and percentage of GPC1$^+$ crExos in PKT mice at indicated age (ANOVA, post-hoc Tamhane T_2, $^{*}P < 0.05$, $^{**}P < 0.01$, $^{***}P < 0.001$ $^{****}P < 0.0001$; 3 technical replicates). **e**, ROC curve analysis of 4-week-old control mice ($n = 6$) and mice with acute pancreatitis ($n = 4$) versus 4-week-old PKT mice ($n = 7$). **f**, Cross-sectional study; blood collected from 16- or 20-day-old control ($n = 6$) and PKT ($n = 7$) mice. **g**, Percentage of GPC1$^+$ crExo beads from control and PKT (16–20-day-old) mice (paired two-tailed Student's t-test, $^{****}P < 0.0001$; 3 technical replicates). **h**, Graphical representation of correlation between histopathological score and GPC1$^+$ crExo levels. **i**, Graphical representation of correlation between age of PKT mice and GPC1$^+$ crExo levels. **j**, Relative percentage of PanIN lesions and representative haematoxylin and eosin (H&E) staining for phosphorylated ERK. Data are mean ± s.d.

pre-PanIN to early PanIN lesions (Fig. 4f, Extended Data Fig. 7a and Extended Data Table 3). GPC1$^+$crExos were detected in all PKT mice (PKT: 8.3% average, control: 1.8% average; Fig. 4g and Extended Data Table 1b). Histological analysis of PKT mice confirmed pre-PanIN lesions in 4 out of 7 PKT mice, and despite no observed histological lesions in 3 out of 7 PKT mice, GPC1$^+$ crExos predicted future pancreatic cancer emergence (Extended Data Table 1b). Moreover, we did not observe pancreas-associated masses by MRI in 16- and 20-day-old PKT mice. Both the histopathological score and age of PKT mice correlated with GPC1$^+$ crExo levels (Fig. 4h, i). In 4 out of 7 PKT mice with no observed histological lesions, downstream signals for Kras activation, such as phosphorylated ERK (pERK), were detected in the pancreas tissue (Fig. 4j and Extended Data Fig. 7a). We also observed exclusive detection of mutant *Kras*^{G12D} mRNA in GPC1$^+$ crExos compared to GPC1$^-$ crExos (Extended Data Fig. 7b).

Discussion

Tumour exosomes are enriched in GPC1, and GPC1$^+$ crExos contain mutant *KRAS* mRNA. We show that GPC1$^+$crExos are a reliable biomarker for detection of early pancreatic cancer. GPC1$^+$crExos are a prognostic marker superior to CA19-9. GPC1$^+$ crExos lead MRI as they can be detected in circulation before MRI-detectable lesions in GEMM of pancreatic cancer.

Routine screening for PDAC using MRI or computed tomography would be prohibitively expensive and associated with a high false-positive rate[27]. GPC1$^+$ crExos detect the possibility of pancreatic cancer in 16-day-old mice with unremarkable pancreatic histology and negative MRI. These results suggest the use of GPC1$^+$ crExos as a detection and monitoring tool for pancreatic cancer, with an emphasis in early detection.

Although *KRAS* mutations are likely driver mutations for pancreatic cancer and are detected in early PanIN-1 lesions, it is estimated that 15–20 years may lapse before early PanIN lesions become metastatic PDAC[28–30]. Nonetheless, PDAC currently presents late with nonspecific clinical symptoms, therefore, as many as 80% of patients present with metastasis at diagnosis[31]. Patients with pancreatic cancer exhibit increased serum levels of CA19-9, carcinoembryonic antigen, CA-50, SPan-1, peanut agglutinin, DU-PAN-2, a-fetoprotein, tissue polypeptide antigen and pancreatic oncofetal antigen[32]. While these markers exhibit some use in tracking biopsy-diagnosed disease, they are also increased in patients with BPD. The lack of specific serum biomarkers and retroperitoneal position of the pancreas challenges the early detection of pancreatic cancer[33,34]. Pancreatico-duodenectomy can be curative if tumours are detected early[35]. Owing to the late diagnosis of pancreatic cancer, only around 15% of patients present with surgically resectable tumours[36]. Studies comparing stage of disease with outcome after surgery suggest that death rates would be reduced if the disease were diagnosed at earlier stages[37].

The isolation of cancer exosomes from patients remains a challenge owing to the lack of specific markers that can distinguish cancer from non-cancer exosomes. Genetic profiling on circulating DNA is cofounded by the fact that the isolated DNA has tumour and non-

tumour origins, thus making mutation detection challenging[38,39]. We previously demonstrated that the DNA in the circulation is mainly associated with exosomes[6]. Therefore, a marker for cancer exosomes will increase the sensitivity of detection for low frequency mutations in the circulation. As a proof-of-concept, GPC1$^+$crExos identified *KRAS* mutations with 100% correlation with *KRAS* mutations in the tumour.

Our results provide evidence for GPC1 as a pan-specific marker of cancer exosomes. GPC1 is a proteoglycan that interacts with many proteins and has diverse functions[40]. Many cancer cells overexpress GPC1, with the most abundant increases observed in pancreatic cancer cells lines and tissue[17–19]. Studies have suggested a role for GPC1 as a positive regulator of cancer progression using orthotopic and GEMMs of PDAC[41,42]. GPC1 is an attractive candidate for detection and isolation of exosomes in the circulation of patients with cancer for genetic and proteomic analysis of specific alterations. Such opportunity offers the possibility for early detection of pancreatic cancer and help in designing potential curative surgical options.

Online Content Methods, along with any additional Extended Data display items and Source Data, are available in the online version of the paper; references unique to these sections appear only in the online paper.

Received 12 September 2014; accepted 22 May 2015.
Published online 24 June 2015.

1. Pan, B. T., Teng, K., Wu, C., Adam, M. & Johnstone, R. M. Electron microscopic evidence for externalization of the transferrin receptor in vesicular form in sheep reticulocytes. *J. Cell Biol.* **101,** 942–948 (1985).
2. Trajkovic, K. *et al.* Ceramide triggers budding of exosome vesicles into multivesicular endosomes. *Science* **319,** 1244–1247 (2008).
3. Skog, J. *et al.* Glioblastoma microvesicles transport RNA and proteins that promote tumour growth and provide diagnostic biomarkers. *Nature Cell Biol.* **10,** 1470–1476 (2008).
4. Al-Nedawi, K. *et al.* Intercellular transfer of the oncogenic receptor EGFRvIII by microvesicles derived from tumour cells. *Nature Cell Biol.* **10,** 619–624 (2008).
5. Demory Beckler, M. *et al.* Proteomic analysis of exosomes from mutant KRAS colon cancer cells identifies intercellular transfer of mutant KRAS. *Mol. Cell Proteomics* **12,** 343–355 (2013).
6. Kahlert, C. *et al.* Identification of double-stranded genomic DNA spanning all chromosomes with mutated KRAS and p53 DNA in the serum exosomes of patients with pancreatic cancer. *J. Biol. Chem.* **289,** 3869–3875 (2014).
7. Ostrowski, M. *et al.* Rab27a and Rab27b control different steps of the exosome secretion pathway. *Nature Cell Biol.* **12,** 19–30 (2010).
8. Théry, C., Ostrowski, M. & Segura, E. Membrane vesicles as conveyors of immune responses. *Nature Rev. Immunol.* **9,** 581–593 (2009).
9. Janowska-Wieczorek, A. *et al.* Microvesicles derived from activated platelets induce metastasis and angiogenesis in lung cancer. *Int. J. Cancer* **113,** 752–760 (2005).
10. Hergenreider, E. *et al.* Atheroprotective communication between endothelial cells and smooth muscle cells through miRNAs. *Nature Cell Biol.* **14,** 249–256 (2012).
11. Lotvall, J. *et al.* Minimal experimental requirements for definition of extracellular vesicles and their functions: a position statement from the International Society for Extracellular Vesicles. *J. Extracell. Vesicles* **3,** 26913 (2014).
12. Taylor, D. D. & Gercel-Taylor, C. Exosomes/microvesicles: mediators of cancer-associated immunosuppressive microenvironments. *Semin. Immunopathol.* **33,** 441–454 (2011).
13. Luga, V. *et al.* Exosomes mediate stromal mobilization of autocrine Wnt-PCP signaling in breast cancer cell migration. *Cell* **151,** 1542–1556 (2012).
14. Théry, C., Amigorena, S., Raposo, G. & Clayton, A. Isolation and characterization of exosomes from cell culture supernatants and biological fluids. *Curr. Protoc. Cell Biol.* **Chapter 3,** Unit–3.22 (2006).
15. Théry, C., Zitvogel, L. & Amigorena, S. Exosomes: composition, biogenesis and function. *Nature Rev. Immunol.* **2,** 569–579 (2002).
16. Wilson, I. D. *et al.* High resolution "ultra performance" liquid chromatography coupled to oa-TOF mass spectrometry as a tool for differential metabolic pathway profiling in functional genomic studies. *J. Proteome Res.* **4,** 591–598 (2005).
17. Matsuda, K. *et al.* Glypican-1 is overexpressed in human breast cancer and modulates the mitogenic effects of multiple heparin-binding growth factors in breast cancer cells. *Cancer Res.* **61,** 5562–5569 (2001).
18. Kleeff, J. *et al.* The cell-surface heparan sulfate proteoglycan glypican-1 regulates growth factor action in pancreatic carcinoma cells and is overexpressed in human pancreatic cancer. *J. Clin. Invest.* **102,** 1662–1673 (1998).
19. Su, G. *et al.* Glypican-1 is frequently overexpressed in human gliomas and enhances FGF-2 signaling in glioma cells. *Am. J. Pathol.* **168,** 2014–2026 (2006).
20. Kahlert, C. & Kalluri, R. Exosomes in tumor microenvironment influence cancer progression and metastasis. *J. Mol. Med.* **91,** 431–437 (2013).
21. Morris, J. P., t., Wang, S. C. & Hebrok, M. KRAS, Hedgehog, Wnt and the twisted developmental biology of pancreatic ductal adenocarcinoma. *Nature Rev. Cancer* **10,** 683–695 (2010).
22. Chen, W. W. *et al.* BEAMing and droplet digital PCR analysis of mutant IDH1 mRNA in glioma patient serum and cerebrospinal fluid extracellular vesicles. *Mol. Ther. Nucleic Acids* **2,** e109 (2013).
23. Del Villano, B. C. *et al.* Radioimmunometric assay for a monoclonal antibody-defined tumor marker, CA 19–9. *Clin. Chem.* **29,** 549–552 (1983).
24. Özdemir, B. C. *et al.* Depletion of carcinoma-associated fibroblasts and fibrosis induces immunosuppression and accelerates pancreas cancer with reduced survival. *Cancer Cell* **25,** 719–734 (2014).
25. Ijichi, H. *et al.* Aggressive pancreatic ductal adenocarcinoma in mice caused by pancreas-specific blockade of transforming growth factor-β signaling in cooperation with active Kras expression. *Genes Dev.* **20,** 3147–3160 (2006).
26. Lee, E. S. & Lee, J. M. Imaging diagnosis of pancreatic cancer: A state-of-the-art review. *World J. Gastroenterol.* **20,** 7864–7877 (2014).
27. Rickes, S., Unkrodt, K., Neye, H., Ocran, K. W. & Wermke, W. Differentiation of pancreatic tumours by conventional ultrasound, unenhanced and echo-enhanced power Doppler sonography. *Scand. J. Gastroenterol.* **37,** 1313–1320 (2002).
28. Murphy, S. J. *et al.* Genetic alterations associated with progression from pancreatic intraepithelial neoplasia to invasive pancreatic tumor. *Gastroenterol.* **145,** 1098–1109 (2013).
29. Bardeesy, N. & DePinho, R. A. Pancreatic cancer biology and genetics. *Nature Rev. Cancer* **2,** 897–909 (2002).
30. Yachida, S. *et al.* Distant metastasis occurs late during the genetic evolution of pancreatic cancer. *Nature* **467,** 1114–1117 (2010).
31. Hidalgo, M. Pancreatic cancer. *N. Engl. J. Med.* **362,** 1605–1617 (2010).
32. Ballehaninna, U. K. & Chamberlain, R. S. Biomarkers for pancreatic cancer: promising new markers and options beyond CA 19–9. *Tumour Biol.* **34,** 3279–3292 (2013).
33. Jazieh, K. A., Foote, M. B. & Diaz, L. A. Jr. The clinical utility of biomarkers in the management of pancreatic adenocarcinoma. *Semin. Radiat. Oncol.* **24,** 67–76 (2014).
34. Locker, G. Y. *et al.* ASCO 2006 update of recommendations for the use of tumor markers in gastrointestinal cancer. *J. Clinical Oncol.* **24,** 5313–5327 (2006).
35. Okano, K. & Suzuki, Y. Strategies for early detection of resectable pancreatic cancer. *World J. Gastroenterol.* **20,** 11230–11240 (2014).
36. Conlon, K. C., Klimstra, D. S. & Brennan, M. F. Long-term survival after curative resection for pancreatic ductal adenocarcinoma. Clinicopathologic analysis of 5-year survivors. *Ann. Surg.* **223,** 273–279 (1996).
37. Bilimoria, K. Y. *et al.* National failure to operate on early stage pancreatic cancer. *Ann. Surg.* **246,** 173–180 (2007).
38. Murtaza, M. *et al.* Non-invasive analysis of acquired resistance to cancer therapy by sequencing of plasma DNA. *Nature* **497,** 108–112 (2013).
39. Yong, E. Cancer biomarkers: Written in blood. *Nature* **511,** 524–526 (2014).
40. David, G. *et al.* Molecular cloning of a phosphatidylinositol-anchored membrane heparan sulfate proteoglycan from human lung fibroblasts. *J. Cell Biol.* **111,** 3165–3176 (1990).
41. Whipple, C. A., Young, A. L. & Korc, M. A KrasG12D-driven genetic mouse model of pancreatic cancer requires glypican-1 for efficient proliferation and angiogenesis. *Oncogene* **31,** 2535–2544 (2012).
42. Aikawa, T. *et al.* Glypican-1 modulates the angiogenic and metastatic potential of human and mouse cancer cells. *J. Clin. Invest.* **118,** 89–99 (2008).

Supplementary Information is available in the online version of the paper.

Acknowledgements Work supported by the Cancer Prevention and Research Institute of Texas and UT MD Anderson Cancer Center. R.K. is also supported by National Institutes of Health (NIH) grants CA-155370, CA-151925, DK 081576 and Metastasis Research Center at the MD Anderson Cancer Center (P30CA016672). V.S.L. is supported by the NIH/NCI under the award number P30CA016672 and the UT MDACC Khalifa Bin Zayed Al Nahya Foundation. D.P.-W. and S.T.G. are supported by the NIH P50-CA094056. Institutional Core Grant CA16672 for High Resolution Electron Microscopy Facility. The Flow Cytometry MDACC core facility is partially funded by NIH P30CA16672. The MDACC Small Animal Imaging Facility is partially funded by NIH grants P30-CA016672 and 5U24-CA126577. S.A.M. is a Human Frontiers Science Program Fellow. C.K. is funded by a Research Fellowship of the Deutsche Forschungsgemeinschaf (DFG). We thank P. A. Kurywchak and S. Kamerkar for the help with the sucrose gradients and K. Dunner Jr for the help with the transmission electron microscopy.

Author Contributions S.A.M. conceptually designed and carried out most of the experiments, generated the data and the figures, and wrote the manuscript; L.B.L. carried out most of the experiments; C.K. performed sequencing of primary tumours, performed most of the statistical analysis of the manuscript and supported manuscript writing; A.F.F. optimized, performed and analysed the UPLC–MS data; S.T.G. performed mouse MRI and analysed the data; J.K. performed the GEMM breeding, bleeding, euthanasia and material collection; V.S.L. performed the GEMM breeding, bleeding, euthanasia, material collection and supported manuscript editing; E.A.M. provided breast cancer patient samples and patient history; J.W., N.R., C.R. and C.P. collected and provided serum samples and patient history for analysis; M.F.F. optimized, performed and analyzed the UPLC–MS data; D.P.-W. performed the mouse MRI interpretation and provided support in data interpretation and analysis; R.K. conceived the idea, conceptually designed the study, supervised the project and wrote the manuscript.

Author Information Reprints and permissions information is available at www.nature.com/reprints. The authors declare no competing financial interests. Readers are welcome to comment on the online version of the paper. Correspondence and requests for materials should be addressed to R.K. (rkalluri@mdanderson.org).

METHODS

Patient samples and tissue collection. The study was conducted according to the Reporting Recommendations for Tumour Marker Prognostic Studies (REMARK) criteria. The studies using human samples were designed as an explorative study. As there was no interventional approach in this study, a priori power calculation was not applicable. Instead, the number of patients included was assessed based on previous studies investigating the diagnostic relevance of circulating biologicals in pancreatic cancer[43].

Serum samples and tissue samples from patients with pancreatic cancer, serum samples only from patients with a benign pancreatic disease and from healthy donors, who had no evidence of acute or chronic or malignant disease and had no surgery within the past 12 months, were received from the department of General, Visceral and Transplantation Surgery from the University of Heidelberg and from the University Hospital of Dresden after approval by the local Institutional Review Board (IRB; Heidelberg: 323/2004, Dresden: EK357112012). The cases were obtained under an IRB-exempt protocol of the MD Anderson Cancer Center (IRB no. PA14-0154). Serum samples from patients with breast cancer were collected at the MD Anderson Cancer Center after approval of the Institutional Review Board (IRB no. LAB10-0690). A written consent for the serum sampling and tumour sampling was obtained pre-operatively from all patients and before serum collection from each healthy donor with disclosure of planned analyses regarding potential prognostic markers. The patients included in this study were all consecutive patients who underwent a surgical procedure at the University Hospital of Heidelberg, Germany, at the University Hospital of Dresden, Germany (pancreatic disease) or at the MD Anderson Cancer Center (breast cancer). All samples were randomly selected from larger cohorts and were analysed in a blinded fashion. Unblinding of clinical parameters and corresponding experimental data was performed only after finishing all experiments. Inclusion criteria of patients were a minimum of 18 years of age, histologically verified pancreatic cancer (pancreatic ductal adenocarcinoma), histologically verified benign pancreatic disease or breast cancer in a resection specimen, and a negative medical history for any other malignant disease. All blood samples were taken before treatment. Inclusion criteria for healthy control donors were a negative medical history for any malignant disease.

On the day of surgery, 10 ml serum separator tubes were used to collect blood samples before surgical incision. The blood samples were then centrifuged at 2,500*g* for 10 min to extract the serum, and the serum was stored at −80 °C until analysed. Likewise, blood samples were collected on day 7 after surgery for 29 patients with PDAC, 4 patients with chronic pancreatitis and 4 patients with an IPMN.

Patient characteristics and clinical specimens. The pancreatic discovery cohort from the University Hospital of Heidelberg included 190 patients with a PDAC, 18 patients with pancreatitis, 8 patients with a benign serous cystadenoma and 5 patients with IPMN. Patients were subjected to surgery between 2006 and 2012 at the Department of General, Visceral, and Transplantation Surgery, University of Heidelberg. Clinical information included age, gender, American Joint Committee on Cancer (AJCC) tumour stage, tumour size (pT), presence and number of lymph node metastases (pN), tumour grade (G), and treatment with (neo-)/adjuvant chemotherapy. The pancreatic cohort from the University Hospital of Dresden included 56 patients with PDAC, 6 patients with chronic pancreatitis, and 20 healthy donors. Patients were subjected to surgery between 2007 and 2013 at the Department of Gastrointestinal, Thoracic and Vascular Surgery, University of Dresden. Clinical information included age, gender, AJCC tumour stage, tumour size (pT), presence and number of lymph node metastases (pN), tumour grade (G), and treatment with (neo-)/adjuvant chemotherapy. The breast cancer cohort consisted of 32 women with breast cancer. All breast cancer patients were treated at the MD Anderson Cancer Center, Houston, Texas. Clinical information included age, gender, AJCC tumour stage, tumour size (pT), presence and number of lymph node metastases (pN), tumour grade, and treatment with (neo-)/adjuvant chemotherapy.

Animal studies. Female nude mice (*nu/nu*) (purchased from Jackson Laboratory) underwent breast pad injections with 0.5 million MDA-MB-231 cells or MDA-MB-231-CD63GFP cells in 20 µl of PBS injected per breast pad. Blood was collected retro-orbitally and exosomes were isolated before injection and at tumour volumes of 300, 550 1,000 and 1,350 mm^3. Mice were euthanized when the tumour size reached 1,500 mm^3 or when severe disease symptoms were present.

The disease progression and genotyping for the $Ptf1a^{cre/+}$; $LSL\text{-}Kras^{G12D/+}$; $Tgfbr2^{L/L}$ (PKT) and the $Pdx1^{cre/+}$; $LSL\text{-}Kras^{G12D/+}$; $p53^{R172H/+}$ (KPC) mice was previously described[32,33] (total of 13 females and 20 males mice). In the PKT longitudinal cohort, retro-orbital blood collections were performed at 4, 5, 6, 7 and 8 weeks of age. Mice were euthanized at 8 weeks of age or sooner if severe disease symptoms were noted. Histopathological analysis of mouse pancreas specimen was performed following previously defined criteria[4]. Four C57BL/6 adult mice were subjected to repeated cerulean injection to induce acute pancreatitis (five hourly repeated intraperitoneal injections of 50 µg cerulein per kilogram of body weight) and euthanized 24 h after injection the last injection. Histological analyses of pancreas of mice was performed according to ref. 44, and a histological score was attributed according to the type of lesions detected: score 1: PanIN1a, score 2: PanIN1 a/b, score 3: PanIN2, score 4: PanIN3, score 5: ductal adenocarcinoma. All mice were housed under standard housing conditions at the MD Anderson Cancer Center (MDACC) animal facilities, and all animal procedures were reviewed and approved by the MDACC Institutional Animal Care and Use Committee.

Cell lines. The following human cells lines were used: HMLE (American Type Culture Collection (ATCC)), MCF10-A (human mammary epithelial cells, ATCC), BJ (ATCC), HDF (human dermal fibroblasts, ATCC), HMEL (human mammary epithelial cells, ATCC), MCF-7 (ATCC), MDA-MB-231 (triple-negative human metastatic breast carcinoma, ATTC), Panc-1 (ATTC), SW480 (ATCC), HCT-116 (ATCC), MIA Paca2 (ATCC) and T3M4 cells (Cell Bank, RIKEN BioResource Centre). The following murine cells lines were used: NIH/3T3 (mouse embryonic fibroblasts, ATCC), E10 (mouse lung epithelial cells, ATCC), NMuMG (ATTC), 4T1 (ATTC) and B16F10 cells (ATTC). All cell lines have been tested for mycoplasma contamination. HDF cells were cultured in DMEM supplemented with 20% (v/v) FBS, 100 U ml^{-1} penicillin and 100 µg ml^{-1} streptomycin. HMLE cells and MCF10A cells were grown in DMEM/F12 supplemented with 5% (v/v) horse serum, 100 U ml^{-1} penicillin, 100 µg ml^{-1} streptomycin, 20 ng ml^{-1} EGF, 0.5 mg ml^{-1} hydrocortisone, 100 ng ml^{-1} cholera toxin and 10 µg ml^{-1} insulin. HMEL, MCF-7, MDA-MB-231, HCT-116, SW480, 4T1, NIH/3T3, E10, U87 and B16F10 cells were maintained in DMEM supplemented with 10% (v/v) FBS, 100 U ml^{-1} penicillin and 100 µg ml^{-1} streptomycin. Panc-1, MIA Paca2 and T3M4 cells were cultured in RPMI-1640 supplemented with 10% (v/v) FBS, 100 U ml^{-1} penicillin and 100 µg ml^{-1} streptomycin. NMuMG cells were grown in DMEM supplemented with 10% (v/v) FBS, 100 U ml^{-1} penicillin, 100 µg ml^{-1} streptomycin and 10 µg ml^{-1} insulin. All cell lines were kept in a humidifying atmosphere at 5% CO_2 at 37 °C. MDA-MB-231-CD63–GFP cells were engineered by transfection with a plasmid encoding a CD63–GFP fusion protein expressed under the control of a CMV promoter (p-CMV6-CD63-GFP from Origene, RG217238). Transfections were performed using Lipofectamine 2000 reagent (Invitrogen).

Exosomes isolation from cells. Exosomes were obtained from supernatant of cells as previously described with some modifications[6]. In brief, cells were grown in T225 cm^2 flasks in FBS depleted of exosomes RPMI media until they reached a confluency of 80–90%. Next, the media was collected and centrifuged at 800*g* for 5 min, followed by a centrifugation step of 2,000*g* for 10 min to discard cellular debris. Then, the media was filtered using a 0.2-µm pore filter (syringe filter, 6786-1302, GE Healthcare). The collected media was then ultracentrifuged at 100,000*g* for 2 h at 4 °C. The exosomes pellet was washed with 35 ml PBS, followed by a second step of ultracentrifugation at 100,000*g* for 2 h at 4 °C. Afterwards, the supernatant was discarded. Exosomes used for RNA extraction were resuspended in 500 µl of Trizol; exosomes used for protein extraction were resuspended in 250 µl of lysis buffer (8 M urea, 2.5% SDS, 5 µg ml^{-1} leupeptin, 1 µg ml^{-1} pepstatin and 1 mM phenylmethylsulphonyl fluoride). Exosomes used for flow cytometry analysis (FACS), TEM (see sections below) and immunogold staining were resuspended in 100 µl PBS. Ten microlitres of these exosomes sample were used for NanoSight LM10 (NanoSight Ltd) analysis after dilution 1:100 in PBS.

Exosomes isolation from human serum samples. As previously described, 250 µl of cell-free serum samples were thawed on ice[6]. Serum was diluted in 11 ml PBS and filtered through a 0.2-µm pore filter. Afterwards, the samples were ultracentrifuged at 150,000*g* overnight at 4 °C. Next, the exosomes pellet was washed in 11 ml PBS followed by a second step of ultracentrifugation at 150,000*g* at 4 °C for 2 h. The supernatant was discarded and pelleted exosomes were resuspended in 500 µl of Trizol for RNA analyses; or in 250 µl of lysis buffer (8 M urea, 2.5% SDS, 5 µg ml^{-1} leupeptin, 1 µg ml^{-1} pepstatin and 1 mM phenylmethylsulphonyl fluoride) for protein analyses. Exosomes used for flow cytometry analysis (FACS), TEM (see sections below) and immunogold staining were resuspended in 100 µl PBS. Ten microlitres of this exosomes sample were used for NanoSight LM10 (NanoSight Ltd) analysis after Nano dilution 1:100 in PBS.

Immunogold labelling and electron microscopy. Fixed specimens at an optimal concentration were placed onto a 400-mesh carbon/formvar coated grids and allowed to absorb to the formvar for a minimum of 1 min. For immunogold staining the grids were placed into a blocking buffer for a block/permeabilization step for 1 h. Without rinsing, the grids were immediately placed into the primary antibody at the appropriate dilution overnight at 4 °C (1:300 anti-CD9 ab92726, Abcam and anti-GPC1 PIPA528055, Thermo Scientific). As controls, some of the

grids were not exposed to the primary antibody. The next day, all the grids were rinsed with PBS then floated on drops of the appropriate secondary antibody attached with 10-nm gold particles (AURION) for 2 h at room temperature. Grids were rinsed with PBS and were placed in 2.5% glutaraldehyde in 0.1 M phosphate buffer for 15 min. After rinsing in PBS and distilled water the grids were allowed to dry and stained for contrast using uranyl acetate. The samples were viewed with a Tecnai Bio Twin transmission electron microscope (FEI) and images were taken with an AMT CCD Camera (Advanced Microscopy Techniques).

Sucrose gradient. Sucrose density gradients were performed to purify exosomes. Exosomes were resuspended in 2 ml of HEPES/sucrose stock solution (2.5 M sucrose, 20 mM HEPES/NaOH solution, pH 7.4). The exosomes suspension was overlaid with a linear sucrose gradient (2.0–0.25 M sucrose, 20 mM HEPES/NaOH, pH 7.4) in a SW41 tube (Beckman). The gradients were ultracentrifuged for 16 h at 210,000*g* at 4 °C. Gradient fractions of 1 ml were collected from top to bottom and densities of each fractions were evaluated using a refractometer. Next, the exosomes pellets were washed in PBS followed by a second step of ultracentrifugation at 150,000*g* at 4 °C for 2 h. Exosomes pellets were resuspended in Laemmli buffer and/or PBS for further immunoblot and flow cytometry analysis.

Flow cytometry analysis of exosomes-bound beads. Exosomes were attached to 4-μm aldehyde/sulphate latex beads (Invitrogen) by mixing 30 μg exosomes in a 10 μl volume of beads for 15 min at room temperature with continuous rotation. This suspension was diluted to 1 ml with PBS and left for 30 min rotating at room temperature. The reaction was stopped with 100 mM glycine and 2% BSA in PBS and left rotating for 30 min at room temperature. Exosomes-bound beads were washed once in 2% BSA in PBS and centrifuged for 1 min at 14,800*g*, blocked with 10% BSA with rotation at room temperature for 30 min, washed a second time in 2% BSA and centrifuged for 1 min at 14,800*g*, and incubated with anti-GPC1 (PIPA528055, Thermo-Scientific, 3 μl of antibody in 20 μl of 2% BSA) during 30 min rotating at 4 °C. Beads were centrifuged for 1 min at 14,800*g*, the supernatant was discarded and beads were washed in 2% BSA and centrifuged for 1 min at 14,800*g*. Alexa-488 or Alexa-594-tagged secondary antibodies (Life Technologies, 3 μl of antibody in 20 μl of 2% BSA) were used during 30 min with rotation at 4 °C. Secondary antibody incubation alone was used as control and to gate the beads with $GPC1^+$-bound exosomes. The percentage of positive beads was calculated relative to the total number of beads analysed per sample (100,000 events). This percentage was therein referred to as the percentage of beads with $GPC1^+$ exosomes.

UPLC–MS. Exosomes were mixed with 200 μl of methanol spiked with the internal standard tryptophan-d5. After brief vortex mixing, the samples were incubated for 1 h at −20 °C. After centrifugation at 16,000*g* for 15 min at 4 °C, 190 μl of the supernatants was collected and the solvent removed. The dried extracts were then reconstituted in 15 μl of methanol, of which 10 μl were transferred to microtubes and derivatized. Chromatographic separation and mass spectrometric detection conditions are described in Supplementary Table 2. The mass range, 50–1,000 *m*/*z*, was calibrated with cluster ions of sodium formate. An appropriate test mixture of standard compounds was analysed before and after the entire set of randomized duplicated sample injections, to examine the retention time stability and sensitivity of the LC–MS system throughout the course of the run. Data were processed using the TargetLynx application manager for MassLynx 4.1 software (Waters Corp.). A set of predefined retention time, mass-to-charge ratio pairs (RT-*m*/*z*), corresponding to metabolites included in the analysis are fed into the program. Associated extracted ion chromatograms (mass tolerance window = 0.05 Da) are then peak-detected and noise-reduced in both the LC and MS domains such that only true metabolite related features are processed by the software. A list of chromatographic peak areas is then generated for each sample injection, using the RT-*m*/*z* data pairs (retention time tolerance = 6 s) as identifiers. Normalization factors were calculated for each metabolite by dividing their intensities in each sample by the recorded intensity of the internal standard in that same sample. Visualization of disjoint and overlapping protein data sets was carried out by drawing a VennDiagram of the 5 protein data sets using an R package[45].

CA19-9 human and GPC1 ELISAs. Serum CA19-9 and GPC1 protein levels in patients with pancreatic cancer, pancreatic cancer precursor lesion, or benign pancreatic disease, and in healthy donors were assessed using the Cancer Antigen CA19-9 Human ELISA Kit (Abcam, ab108642) and the GPC1 Human ELISA kit (ABIN840422), according to the manufacturer's directions.

Western blot analyses. Cells were lysed in RIPA buffer containing 5 μg ml^{-1} leupeptin, 1 μg ml^{-1} pepstatin and 1 mM phenylmethylsulphonyl fluoride. Exosomes were lysed in 8 M urea, 2.5% SDS containing 5 μg ml^{-1} leupeptin, 1 μg ml^{-1} pepstatin and 1 mM phenylmethylsulphonyl fluoride. Sample loading was normalized according to Bradford relative protein quantification and proteins separated following an electrophoretic gradient across polyacrylamide gels. Wet electrophoretic transfer was used to transfer the proteins in the gel onto PVDF membranes (ImmobilonP). The protein blot was blocked for 1 h at room temperature with 5% non-fat dry milk in PBS/0,05% Tween and incubated overnight at 4 °C with the following primary antibodies: 1:300 anti-GPC1, PIPA528055 (Thermo-Scientific); 1:300 anti-β-actin A3854 (Sigma-Aldrich); 1:300 anti-CD81 sc-166029 (Santa-Cruz); 1:300 anti-flottilin1 sc-25506 (Santa-Cruz). Afterwards, horseradish peroxidase (HRP)-conjugated secondary antibodies were incubated for 1 h at room temperature. Washes after antibody incubations were done on an orbital shaker, four times at 10-min intervals, with PBS 0.05% Tween20. Blots were developed with chemiluminescent reagents from Pierce.

RNA extraction of cells and exosomes. RNA of cells and exosomes was isolated using Trizol Plus RNA purification kit (Life Technologies, 12183555) according to manufactures protocol. RNA was quantified using a Nanodrop ND-1000 (Thermo Fischer Scientific).

qRT–PCR. Quantitative reverse transcriptase PCR (qRT–PCR) was performed on DNase-treated RNA using the SuperScript III Platinum One-Step Quantitative RT–PCR System (11732-088, Invitrogen) according to the manufacturer's directions on a 7300 Sequence Detector System (Applied Biosystems). 150 ng of RNA extracted from 2.5×10^8 exosomes was used as qPCR input. Primers for $KRAS^{G12D}$ and $KRAS^{G12V}$ mRNA (both Sigma-Aldrich) were designed as reported previously[46]. In brief, the altered base of the $KRAS^{G12D}$ and $KRAS^{G12V}$ mutation was kept at the 3′ end of the forward primer. An additional base mutation was included two positions before the *KRAS* mutation to increase the specificity of the amplification of the mutant *KRAS* allele. Forward primer sequence for $KRAS^{G12D}$ mRNA: F-5′-ACTTGTGGTAGTTGGAGC*A*G*A*-3′ (italicized bases denote mutations corresponding to the *KRAS* mutant). Forward primer sequences for $KRAS^{G12V}$ mRNA: F-5′-ACTTGTGGTAGTTGGAGC*AGT*-3′. Forward primer sequences for *KRAS* wild-type mRNA: F-5′-ACTTGTGGTAGTTGGAGCTGG-3′. Reverse primer for all *KRAS* mRNAs: R-5′-TTGGATCATATTCGTCCACAA-3′. *GPC1* mRNA primer pairs (PPH06045A) and 18S mRNA primer pairs (QF00530467) were purchased as ready specific primer pairs from Qiagen. Threshold cycle[47] (C_t) the fractional cycle number at which the amount of amplified target reached a fixed threshold, was determined and expression was measured using the $2^{-\Delta C_t}$ formula, as previously reported[48].

DNA extraction from human primary pancreatic cancer tumours and crExos. Immediately after resection, pancreatic tumour samples were snap-frozen in liquid nitrogen and stored at −80 °C until further processing. A 10-μm reference section of each sample was cut and stained with haematoxylin and eosin by standard methods to evaluate the proportion of tumour tissue and adjacent tumour stroma. Samples with a tumour stroma proportion >30% were excluded into this study. DNA isolation was performed using a commercial DNA Extraction Kit (DNeasy Blood & Tissue Kit, 69506, Qiagen) according to the manufacturer's protocol. The amount of DNA from tumour samples was quantified using a Nanodrop 1000 Spectrophotometer (Thermo Fisher Scientific).

PCR and Sanger sequencing. PCR was performed in a 25-μl reaction tube consisting of 10 μl template DNA, 1 μM of each primer, 2.5 mM dNTP, 2.5 μl 10× PCR buffer, 25 mM Mg solution, 0.5 μl H_2O and 2.5 μl Taq polymerase. Amplification was carried out in a T100 ThermoCycler (Bio-Rad) under the following conditions: 94 °C for 1 min, 2 cycles of 94 °C for 10 s, 67 °C for 30 s, 70 °C for 30 s; 2 cycles of 94 °C for 10 s, 64 °C for 30 s, 70 °C for 30 s; 2 cycles of 94 °C for 10 s, 61 °C for 30 s, 70 °C for 30 s; 35 cycles of 94 °C for 10 s, 59 °C for 30 s, 70 °C for 30 s; endless 4 °C. *KRAS* amplicon were generated using the following primers: forward 5′-AAGGCCTGCTGAAAATGACTG-3′, 5′-AGAATGGTCCTGCACCAGTAA-3′. PCR products were purified using the QIAquick PCR purification kit (Qiagen). Subsequently, sequencing reaction was performed using BigDye terminator kit (v3.1, Life Technologies) according to the manufacturer's instructions. Sequencing products were separated on an ABI 3730 automated sequencer (Life Technologies). KRAS mutation status was evaluated using Finch TV (Geospiza, Inc.).

MRI imaging. MRI studies were conducted using a 7T small animal MR system, the Biospec USR70/30 (Bruker Biospin MRI) is based on an actively shielded 7T magnet with a 30-cm bore and cryo-refrigeration. The system is equipped with 6 cm inner-diameter gradients that deliver a maximum gradient field of 950 mT m^{-1}. A 3.5 cm inner-diameter linear birdcage coil transmits and receives the MR signal. For image acquisition, T2-weighted, respiratory gated, multi-slice imaging will be performed with respiration held to under 25 breaths per minute to minimize motion artefacts in the abdomen. For mice where fat signal might mask the T2 weighted image the fat-suppression pulse module will be used. Acquisition parameters were minimally modified from ref. 49. The rapid acquisition with relaxation enhancement (RARE) T2-weighted pulse sequence was modified to include an effective Te (time of echo) of 56 ms with a total TR (time repetition) of 2,265 ms. Between 18 and 20 coronal slices were acquired per mouse with a slice thickness of 0.75 mm and slice spacing of 1 mm. In plane, pixel sizes of 0.156 mm × 0.156 mm with a matrix size of 256 × 192 (40 mm × 30 mm FOV)

was chosen to minimize in plane partial volume effects, maintain a FOV sufficient to cover the abdomen, while also providing sufficient throughput for the experiment.

To measure tumour burden, the region of suspected lesions are drawn blinded on each slice after images intensities were normalized. The volume is calculated by addition of delineated region of interest in $mm^2 \times 1$ mm slice distance.

Statistical analysis. The GraphPad Prism version 6.0 (GraphPad Software) and MedCalc statistical software version 13.0 (MedCalc Software bvba) were used for all calculations. Unpaired Student's *t*-test was applied to calculate expression differences of the qPCR results (ΔC_t values). ANOVA tests were performed to calculate differences of multiple serum factors in murine and human serum samples. As a post-hoc test, a Tukey–Kramer test was applied for pairwise comparison of subgroups when the ANOVA test was positive in case of equal variance. Tamhane T_2 test was applied for pairwise comparison of subgroups when the ANOVA test was positive in case of unequal variances. A paired two-tailed Student's *t*-test was applied to assay differences in the percentage of beads with $GPC1^+$ crExos and CA19-9 in the longitudinal cohort between pre-operative and postoperative blood samples. ROC curves were used to determine the sensitivity, specificity, positive and negative predictive values and to compare AUCs of serum factors using the Delong method[50]. The cut-off value was determined using the Youden index. Univariate analysis using the log-rank test was conducted to visualize (Kaplan–Meier curves) and assess disease-specific survival (time from diagnosis to cancer-related death or last follow-up) in the longitudinal cohort of patients with pancreatic cancer. A multivariate analysis using the Cox proportional hazards regression model was performed to evaluate the effect of a decrease of the percentage of beads with $GPC1^+$ crExos in addition to age (continuous variable), AJCC tumour stage, and tumour grade (G) and CA19-9 levels ($U\,ml^{-1}$). Correlation analysis between murine tumour burden and percentage beads with $GPC1^+$ crExos was performed using the Spearman correlation test. Figures were prepared using GraphPad Prism and MedCalc statistical software version 13.0. All presented *P* values are two-sided and $P < 0.05$ was considered to be statistically significant.

43. Brand, R. E. *et al.* Serum biomarker panels for the detection of pancreatic cancer. *Clin. Cancer Res.* **17,** 805–816 (2011).
44. Hingorani, S. R. *et al.* Preinvasive and invasive ductal pancreatic cancer and its early detection in the mouse. *Cancer Cell* **4,** 437–450 (2003).
45. Chen, H. & Boutros, P. C. VennDiagram: a package for the generation of highly-customizable Venn and Euler diagrams in R. *BMC Bioinformatics* **12,** 35 (2011).
46. Rachagani, S. *et al.* Activated $Kras^{G12D}$ is associated with invasion and metastasis of pancreatic cancer cells through inhibition of E-cadherin. *Br. J. Cancer* **104,** 1038–1048 (2011).
47. Rothstein, D. M. *et al.* Targeting signal 1 through CD45RB synergizes with CD40 ligand blockade and promotes long term engraftment and tolerance in stringent transplant models. *J. Immunol.* **166,** 322–329 (2001).
48. Livak, K. J. & Schmittgen, T. D. Analysis of relative gene expression data using real-time quantitative PCR and the $2^{-\Delta\Delta C}{}_T$ method. *Methods* **25,** 402–408 (2001).
49. Schmid, A., Braumuller, H., Wehrl, H. F., Rocken, M. & Pichler, B. J. Non-invasive monitoring of pancreatic tumor progression in the RIP1-Tag2 mouse by magnetic resonance imaging. *Mol. Imaging Biol.* **15,** 186–193 (2013).
50. DeLong, E. R., DeLong, D. M. & Clarke-Pearson, D. L. Comparing the areas under two or more correlated receiver operating characteristic curves: a nonparametric approach. *Biometrics* **44,** 837–845 (1988).

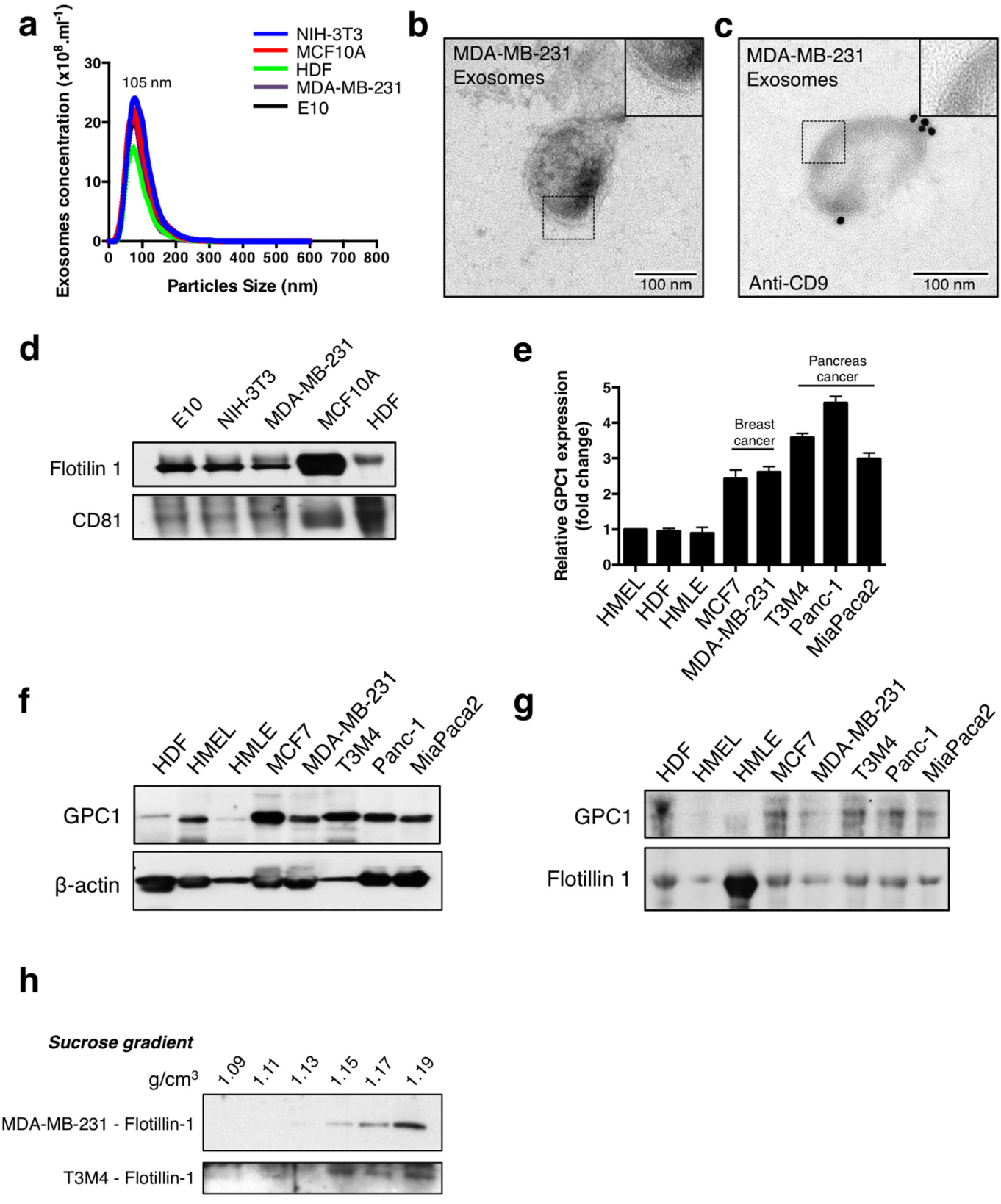

Extended Data Figure 1 | Exosome isolation. **a**, Exosome concentration and size distribution by NanoSight analysis of culture supernatant from NIH/3T3, MCF10A, HDF, MDA-MB-231 and E10 cells. Size mode: 105 nm (3 technical replicates). **b**, TEM micrograph of MDA-MB-231-derived exosomes. Top right image shows a digitally zoomed inset. **c**, TEM micrograph of MDA-MB-231-derived exosomes following immunogold labelling for CD9. Gold particles are depicted as black dots. Top right image shows a digitally zoomed inset. **d**, Immunoblot of flotillin1 and CD81 in exosomal proteins extracted from culture supernatant of E10, NIH/3T3, MDA-MB-231, MCF10A and HDF cells. **e**, qRT–PCR measurement of *GPC1* mRNA levels in HMEL, HDF, HMLE, MCF7, MDA-MB-231, T3M4, Panc-1 and MIA Paca2 cells. Results are mean ± s.d.; $n = 3$, 3 biological replicates, with 3 technical replicates each. **f**, Immunoblot of GPC1 in HMEL, HDF, HMLE, MCF7, MDA-MB-231, T3M4, Panc-1 and MIA Paca2 cell lysates (top). β-actin was used as a loading control (bottom). **g**, Immunoblot of GPC1 in exosomal protein lysates derived from the culture supernatant of 3 non-tumorigenic cell lines (HDF, HMEL and HMLE) and 5 tumorigenic cell lines (MCF7, MDA-MB-231, T3M4, Panc-1 and MIA Paca2) (top). Flotillin1 was used as loading control (bottom). **h**, Immunoblot of flotillin1 in exosomal protein lysates from the culture supernatant of MDA-MB-231 and T3M4 following sucrose gradient purification. The protein content is assayed in each of the density layers listed.

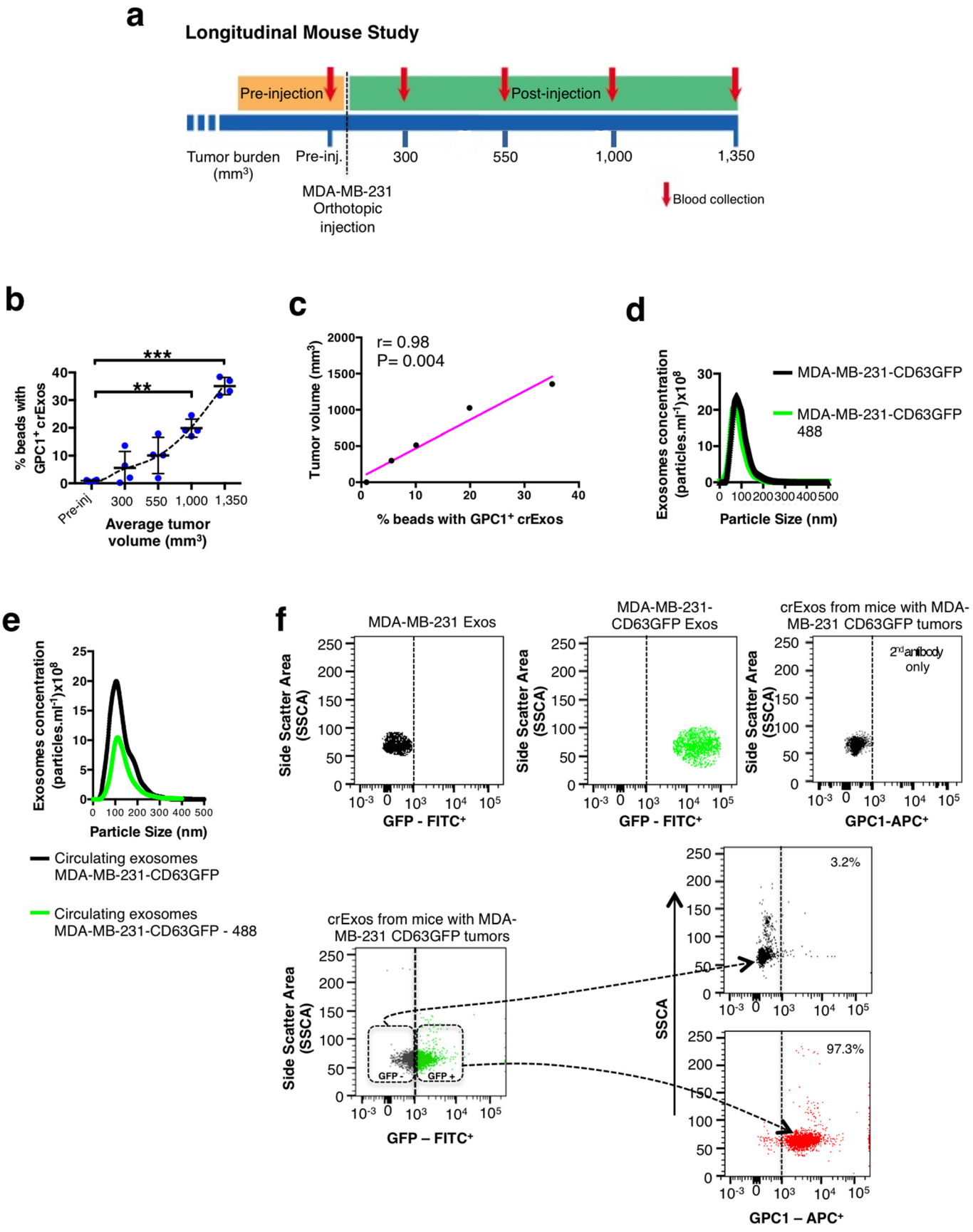

Extended Data Figure 2 | GPC1$^+$ crExos are derived from cancer cells in tumour-bearing mice. **a**, Longitudinal blood collection; nude mice with orthotopic MDA-MB-231 tumours ($n = 4$ mice). **b**, Percentage of beads with GPC1$^+$ crExos plotted against average tumour volume ($n = 4$ mice, each sample analysed in technical triplicates for GPC1). ANOVA, post-hoc Tamhane T_2, $^{**}P < 0.01$, $^{***}P < 0.001$. Data are mean ± s.d. **c**, Correlation between tumour volume and the percentage of beads with GPC1$^+$ crExos (Pearson correlation test). **d**, NanoSight of exosomes from MDA-MB-231-CD63–GFP cells. Black: all exosomes; green: CD63–GFP$^+$ exosomes ($n = 3$ technical replicates). **e**, NanoSight of crExos from mice with a MDA-MB-231-CD63–GFP orthotopic tumour. Black: all exosomes; green: CD63–GFP$^+$ exosomes ($n = 3$ technical replicates). **f**, FACS analysis of beads with exosomes from cultured MDA-MB-231 (top left) and MDA-MB-231-CD63–GFP (top middle) cells, and crExos of mice with MDA-MB-231-CD63–GFP orthotopic tumours (bottom left). Staining of CD63–GFP$^+$ (cancer-cell-derived) and CD63–GFP$^-$ (host-derived) crExos for GPC1 (allophycocyanin (APC)$^+$ bottom right; $n = 3$ biological replicates and 3 technical replicates). The percentage of positive beads is listed. Negative control: secondary antibody alone (top right).

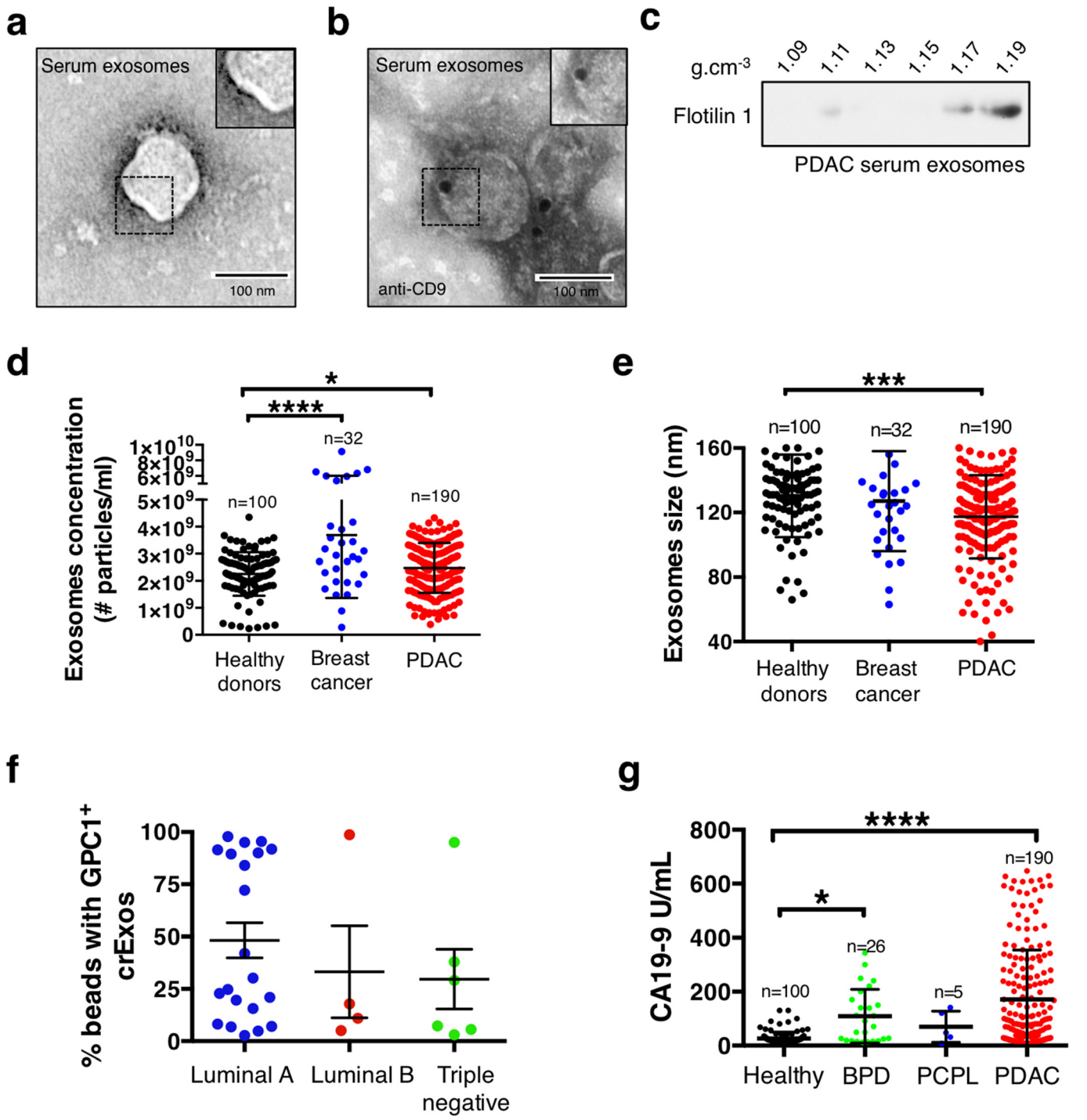

Extended Data Figure 3 | NanoSight analysis in human serum samples. **a**, TEM micrograph of serum-derived exosomes from a cancer patient. Top right image shows a digitally zoomed inset. **b**, TEM micrograph of serum-derived exosomes from a cancer patient after immunogold labelling for CD9. Gold particles are depicted as black dots. Top right image shows a digitally zoomed inset. **c**, Immunoblot of flotillin1 of exosomal protein lysates from serum of cancer patient following exosome purification by a sucrose gradient. The protein content is assayed in each of the density layers listed. **d**, Exosome concentration by NanoSight analysis showing the number of exosomes per millilitre of serum derived from healthy donors ($n = 100$), breast cancer patients ($n = 32$) and patients with PDAC ($n = 190$) (ANOVA, post-hoc Tamhane T_2, $^*P < 0.05$, $^{****}P < 0.0001$; 3 technical replicates). **e**, Exosomes size distribution by NanoSight analysis showing the mode size of exosomes in 1 ml of serum derived from healthy donors ($n = 100$), breast cancer patients ($n = 32$) and patients with PDAC ($n = 190$) (ANOVA, post-hoc Tukey–Kramer test, $^{***}P < 0.001$; 3 technical replicates). **f**, Scatter dot plots depicting the percentage of beads with $GPC1^+$-bound exosomes purified from the serum of breast cancer patients. The patients are subdivided into three subtypes: luminal A, luminal B and triple-negative breast cancer. **g**, Scatter plots depicting the serum CA19-9 concentration (U ml^{-1}), evaluated by ELISA, in healthy donors ($n = 100$), patients with BPD ($n = 26$), PCPL ($n = 5$) and PDAC ($n = 190$). Discovery cohort, ANOVA, post-hoc Tamhane T_2, $^*P < 0.05$; $^{****}P < 0.0001$; 3 technical replicates. Data are mean ± s.d.

a

Parameter	AUC	CI	Cut-off value	Sensitivity	95% CI	Specificity	95% CI2
Beads with GPC1+ crExos (%)	1	0.988 - 1.000	>7.6	100	98.1 - 100.0	100	97.1 - 100.0
CA 19-9 (U/ml)	0.739	0.687 - 0.787	>26.3063	76.84	70.2 - 82.6	64.29	55.3 - 72.6
Exosomes Concentration (^10E09)	0.57	0.513 - 0.625	>32.8	25.79	19.7 - 32.6	92.06	85.9 - 96.1
Exosome Size (nm)	0.676	0.621 - 0.727	≤122	63.16	55.9 - 70.0	70.63	61.9 - 78.4

b

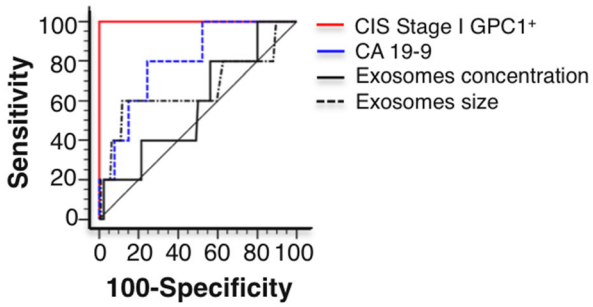

Parameter	AUC	CI	Cut-off value	Sensitivity	95% CI	Specificity	95% CI
GPC-1-positive exosomes (%)	1	0.972 - 1.000	>7.6	100	47.8 - 100.0	100	97.1 - 100.0
CA 19-9 (U/ml)	0.735	0.651 - 0.808	>30.8435	80	28.4 - 99.5	66.67	57.7 - 74.8
Exosomes Concentration (^10E09)	0.581	0.492 - 0.667	≤23.75E08	60	14.7 - 94.7	43.65	34.8 - 52.8
Exosomes Size (nm)	0.663	0.576 - 0.744	≤107	60	14.7 - 94.7	88.1	81.1 - 93.2

c

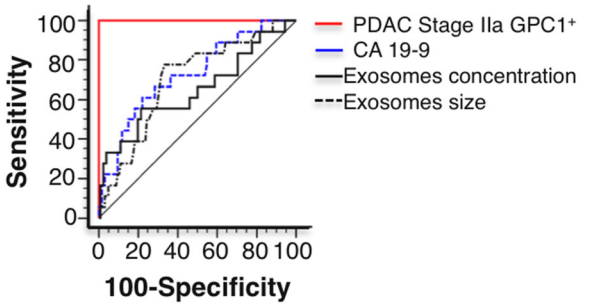

Parameter	AUC	CI	Cut-off value	Sensitivity	95% CI	Specificity	95% CI
GPC-1-positive exosomes (%)	1	0.975 - 1.000	>7.6	100	81.5 - 100.0	100	97.1 - 100.0
CA 19-9 (U/ml)	0.668	0.585 - 0.744	>26.3063	66.67	41.0 - 86.7	64.29	55.3 - 72.6
Exosomes Concentration (^10E09)	0.648	0.564 - 0.726	>28.1E08	55.56	30.8 - 78.5	78.57	70.4 - 85.4
Exosomes Size (nm)	0.7	0.619 - 0.774	≤124	77.78	52.4 - 93.6	66.67	57.7 - 74.8

d

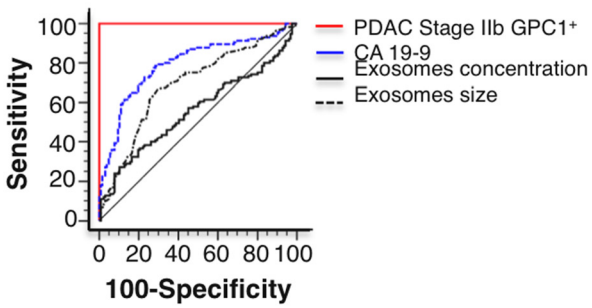

Parameter	AUC	CI	Cut-off value	Sensitivity	95% CI	Specificity	95% CI
GPC-1-positive exosomes (%)	1	0.985 - 1.000	>7.6	100	96.9 - 100.0	100	97.1 - 100.0
CA 19-9 (U/ml)	0.74	0.680 - 0.794	>25.3562	79.49	71.0 - 86.4	63.49	54.4 - 71.9
Exosomes Concentration (^10E09)	0.559	0.494 - 0.622	>31.7E08	27.35	19.5 - 36.4	89.68	83.0 - 94.4
Exosomes Size (nm)	0.692	0.630 - 0.749	≤122	66.67	57.4 - 75.1	70.63	61.9 - 78.4

e

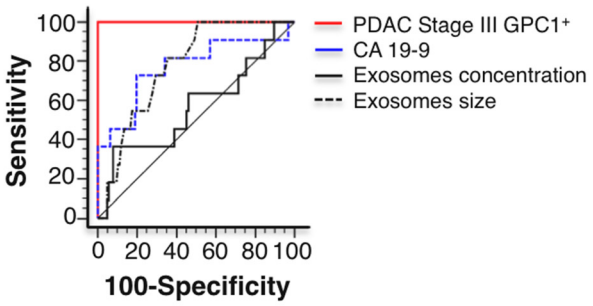

Parameter	AUC	CI	Cut-off value	Sensitivity	95% CI	Specificity	95% CI
GPC-1-positive exosomes (%)	1	0.973 - 1.000	>7.6	100	71.5 - 100.0	100	97.1 - 100.0
CA 19-9 (U/ml)	0.729	0.646 - 0.801	>36.1015	72.73	39.0 - 94.0	71.43	62.7 - 79.1
Exosomes Concentration (^10E09)	0.566	0.478 - 0.650	>32.8E08	36.36	10.9 - 69.2	92.06	85.9 - 96.1
Exosomes Size (nm)	0.776	0.697 - 0.842	≤132	100	71.5 - 100.0	49.21	40.2 - 58.3

f

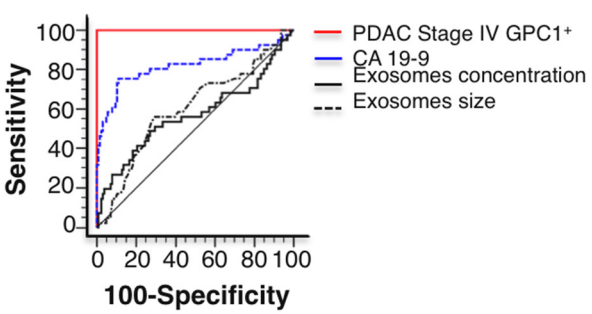

Parameter	AUC	CI	Cut-off value	Sensitivity	95% CI	Specificity	95% CI
GPC-1-positive exosomes (%)	1	0.978 - 1.000	>7.6	100	91.4 - 100.0	100	97.1 - 100.0
CA 19-9 (U/ml)	0.788	0.718 - 0.848	>61.2284	75.61	59.7 - 87.6	78.57	70.4 - 85.4
Exosomes Concentration (^10E09)	0.569	0.490 - 0.645	>26.5E08	51.22	35.1 - 67.1	70.63	61.9 - 78.4
Exosomes Size (nm)	0.604	0.525 - 0.678	≤122	56.1	39.7 - 71.5	70.63	61.9 - 78.4

g

Parameter	AUC	CI	Cut-off value	Sensitivity	95% CI	Specificity	95% CI2
Beads with GPC1+ crExos (%)	1	0.956 - 1.000	>12	100	93.6 - 100.0	100	86.8 - 100.0
Exosomes Concentration (^10E09)	0.714	0.603 - 0.808	>22.2E08	51.79	38.0 - 65.3	84.62	65.1 - 95.6
Exosome Size (nm)	0.648	0.534 - 0.750	≤121	62.5	48.5 - 75.1	65.38	44.3 - 82.8

Extended Data Figure 4 | Tumour-stage-specific analysis. **a**, Table associated with ROC curve analysis depicted in Fig. 1f. **b**–**f**, ROC curve analysis for the percentage of $GPC1^{+}$ crExos (red line), CA19-9 serum levels (blue scattered line), exosome concentration (black line) and exosome size (scattered black line) in patients with carcinoma *in situ* (CIS) or stage I pancreatic cancer ($n = 5$) (**a**), stage IIa pancreatic cancer ($n = 18$) (**b**), stage IIb pancreatic cancer ($n = 117$) (**c**), stage III pancreatic cancer ($n = 11$) (**d**), and stage IV pancreatic cancer ($n = 41$) (**e**), compared to healthy donors ($n = 100$) and patients with a benign pancreatic disease ($n = 26$), total $n = 126$. **g**, Table associated with ROC curve analysis depicted in Fig. 1h. CI, confidence interval.

a

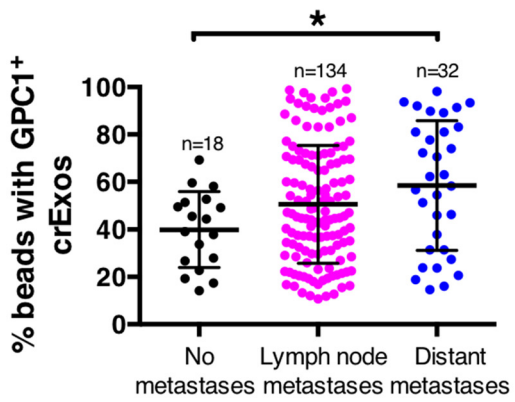

b

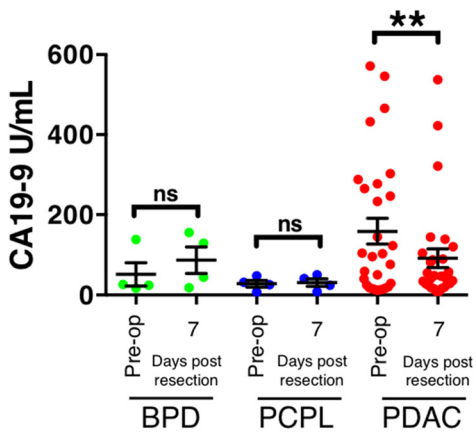

c

Multivariate analysis – overall survival

Parameter	Hazard ratio	95% CI	P - Value
GPC1 drop between day 0 and day 7	5.511	1.697-17.892	0.005
Age	0.96	0.898-1.026	0.227
AJCC stage	1.203	0.429-3.374	0.726
Tumor grade	1.024	1.004-1.044	0.018
CA 19-9 drop between day 0 and day 7	2.453	0.885-6.796	0.084

d

Multivariate analysis – disease specific survival

Parameter	Hazard ratio	95% CI	P - Value
GPC1 drop between day 0 and day 7	5.353	1.651-17.358	0.005
Age	0.962	0.899-1.028	0.254
AJCC stage	1.177	0.428-3.237	0.752
Tumor grade	1.016	0.992-1.041	0.197
CA 19-9 drop between day 0 and day 7	2.138	0.762-5.993	0.149

e

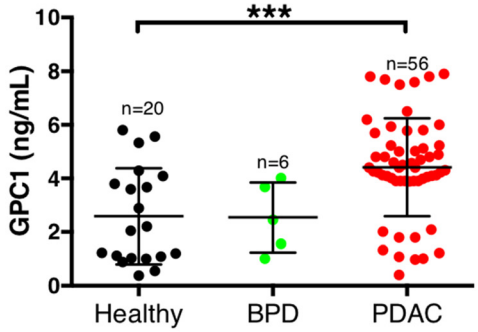

f

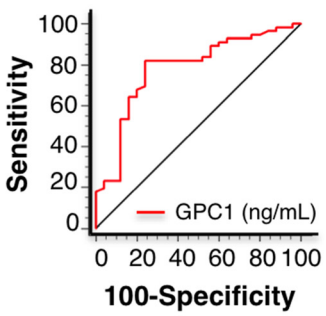

Parameter	AUC	CI	Cut-off value	Sensitivity	95% CI	Specificity	95% CI
GPC-1 ELISA (ng/ml)	0.781	0.675 - 0.865	>3.8	82.14	69.6 - 91.1	76	54.9 - 90.6

Extended Data Figure 5 | Longitudinal human study. **a**, Scatter plots of the percentage of beads with $GPC1^{+}$ crExos by flow cytometry in patients with pancreatic cancer. Patients are divided based on metastatic disease (non-metastatic lesions, lymph node metastases and distant metastases) (ANOVA, post-hoc Tukey–Kramer test, $^{*}P < 0.05$; 3 technical replicates). **b**, Scatter plots depicting serum CA19-9 levels (U ml^{-1}) in patients with BPD ($n = 4$), PCPL ($n = 4$) and PDAC ($n = 29$) on the pre-operative day and post-operative day 7 in patients (paired two-tailed Student's *t*-test, $^{**}P < 0.01$; 3 technical replicates). **c**, **d**, Multivariate analysis (Cox proportional hazards regression model) of prognostic parameters for overall (**c**) and disease-specific (**d**) survival of patients with pancreatic cancer in the longitudinal cohort ($n = 29$). **e**, Scatter plots depicting serum GPC1 (ng ml^{-1}) levels by ELISA in patients with BPD ($n = 6$), PDAC ($n = 56$) and healthy controls ($n = 20$) (ANOVA, post-hoc Tukey–Kramer test, $^{****}P < 0.0001$; 3 technical replicates). **f**, ROC curve for circulating GPC1 protein (red line) in patients with pancreatic cancer ($n = 56$) versus healthy donors ($n = 20$) and patients with a benign pancreatic disease ($n = 26$), total $n = 6$.

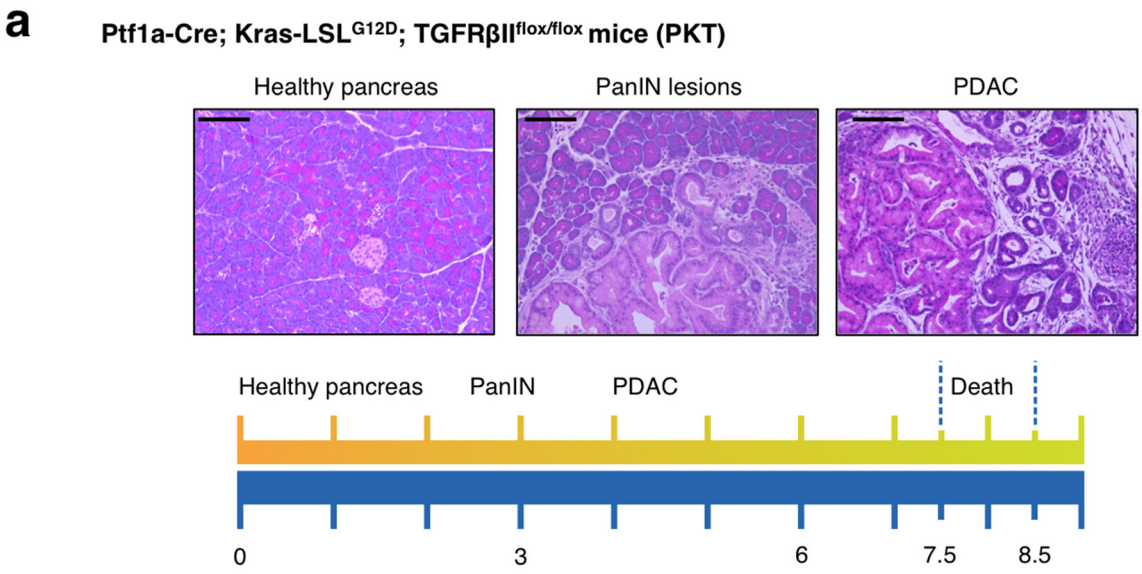

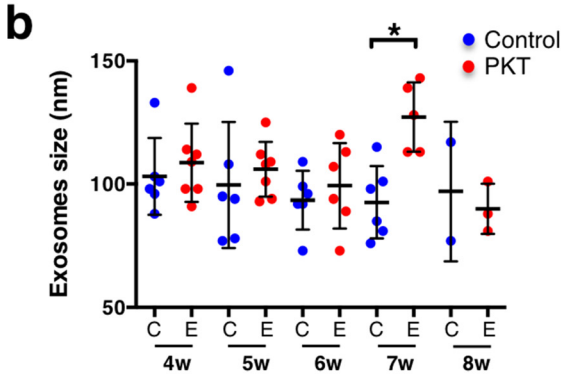

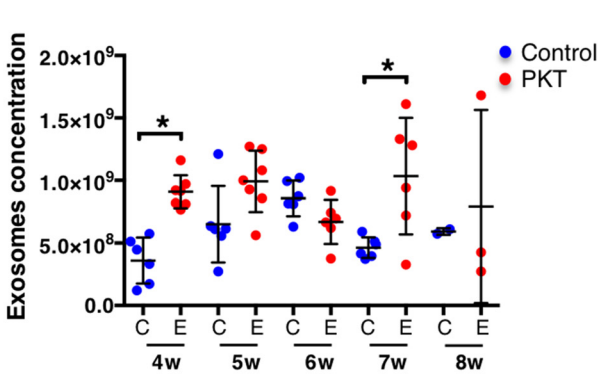

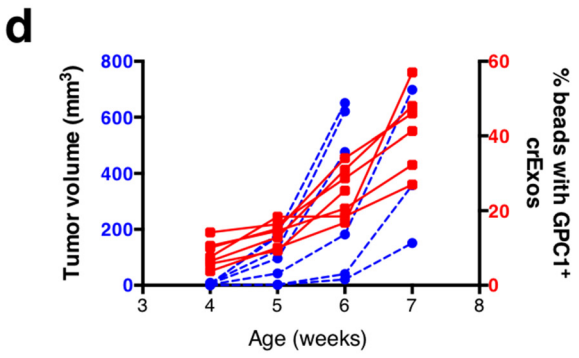

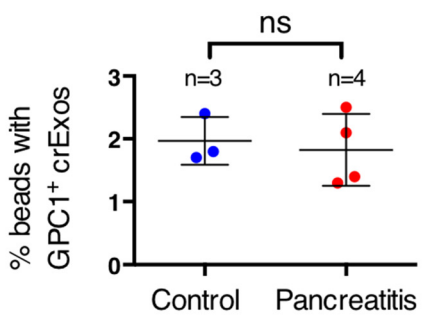

f

4 weeks

Parameter	AUC	CI	Cut-off value	Sensitivity	95% CI	Specificity	95% CI
GPC-1-positive exosomes (%)	1	0.805 - 1.000	>2.5	100	59.0 - 100.0	100	69.2 - 100.0
Exosomes Concentration (^10E08)	0.814	0.555 - 0.958	>5.76	100	59.0 - 100.0	70	34.8 - 93.3
Exosomes Size (nm)	0.657	0.393 - 0.865	>104	57.14	18.4 - 90.1	80	44.4 - 97.5

5 weeks

Parameter	AUC	CI	Cut-off value	Sensitivity	95% CI	Specificity	95% CI
GPC-1-positive exosomes (%)	1	0.794 - 1.000	>3.6	100	59.0 - 100.0	100	66.4 - 100.0
Exosomes Concentration (^10E08)	0.714	0.440 - 0.906	>8.02	85.71	42.1 - 99.6	60	26.2 - 87.8
Exosomes Size (nm)	0.746	0.472 - 0.925	>82	100	59.0 - 100.0	40	12.2 - 73.8

6 weeks

Parameter	AUC	CI	Cut-off value	Sensitivity	95% CI	Specificity	95% CI
GPC-1-positive exosomes (%)	1	0.794 - 1.000	>2.6	100	54.1 - 100.0	100	69.2 - 100.0
Exosomes Concentration (^10E08)	0.783	0.512 - 0.945	≤743000000	83.33	35.9 - 99.6	80	44.4 - 97.5
Exosomes Size (nm)	0.592	0.324 - 0.824	>104	50	11.8 - 88.2	80	44.4 - 97.5

7 weeks

Parameter	AUC	CI	Cut-off value	Sensitivity	95% CI	Specificity	95% CI
GPC-1-positive exosomes (%)	1	0.794 - 1.000	>2.5	100	54.1 - 100.0	100	69.2 - 100.0
Exosomes Concentration (^10E08)	0.725	0.451 - 0.913	>11.64	50	11.8 - 88.2	100	69.2 - 100.0
Exosomes Size (nm)	0.933	0.692 - 0.998	>104	100	54.1 - 100.0	80	44.4 - 97.5

Extended Data Figure 6 | PDAC GEMM longitudinal study. **a**, Schematic diagram depicting the spontaneous development and progression of pancreatic cancer in PKT mice, and haematoxylin and eosin of the pancreas at the indicated time points showing healthy pancreas, and PanIN and PDAC lesions. Scale bars, 100 μm. **b**, **c**, Exosome size (**b**) and concentration (**c**) assayed by NanoSight analysis from the serum of PKT mice (E: experimental, red) and control mice (C: control, blue) at 4, 5, 6, 7 and 8 weeks of age (ANOVA, post-hoc Tukey–Kramer test, $*P < 0.05$; 3 technical replicates). **d**, Graph depicting the time-wise progression of tumour volume measured by MRI and the percentage of $GPC1^+$-bound crExo beads in individual PKT mice (blue: tumour volume, red: percentage of $GPC1^+$ crExos). **e**, Percentage of $GPC1^+$ crExo beads from control mice ($n = 3$) and mice with cerulein-induced acute pancreatitis ($n = 4$) (two-tailed Student's *t*-test, ns: not significant; 3 technical replicates). **f**, Results from ROC curves for the percentage of $GPC1^+$-bound crExo beads, exosome concentration and size in 4-, 5-, 6- and 7-week-old PKT mice ($n = 7$) versus control (including age-matched littermate healthy control ($n = 6$) and mice with induced acute pancreatitis ($n = 4$), $n = 10$)). Data are mean ± s.d.

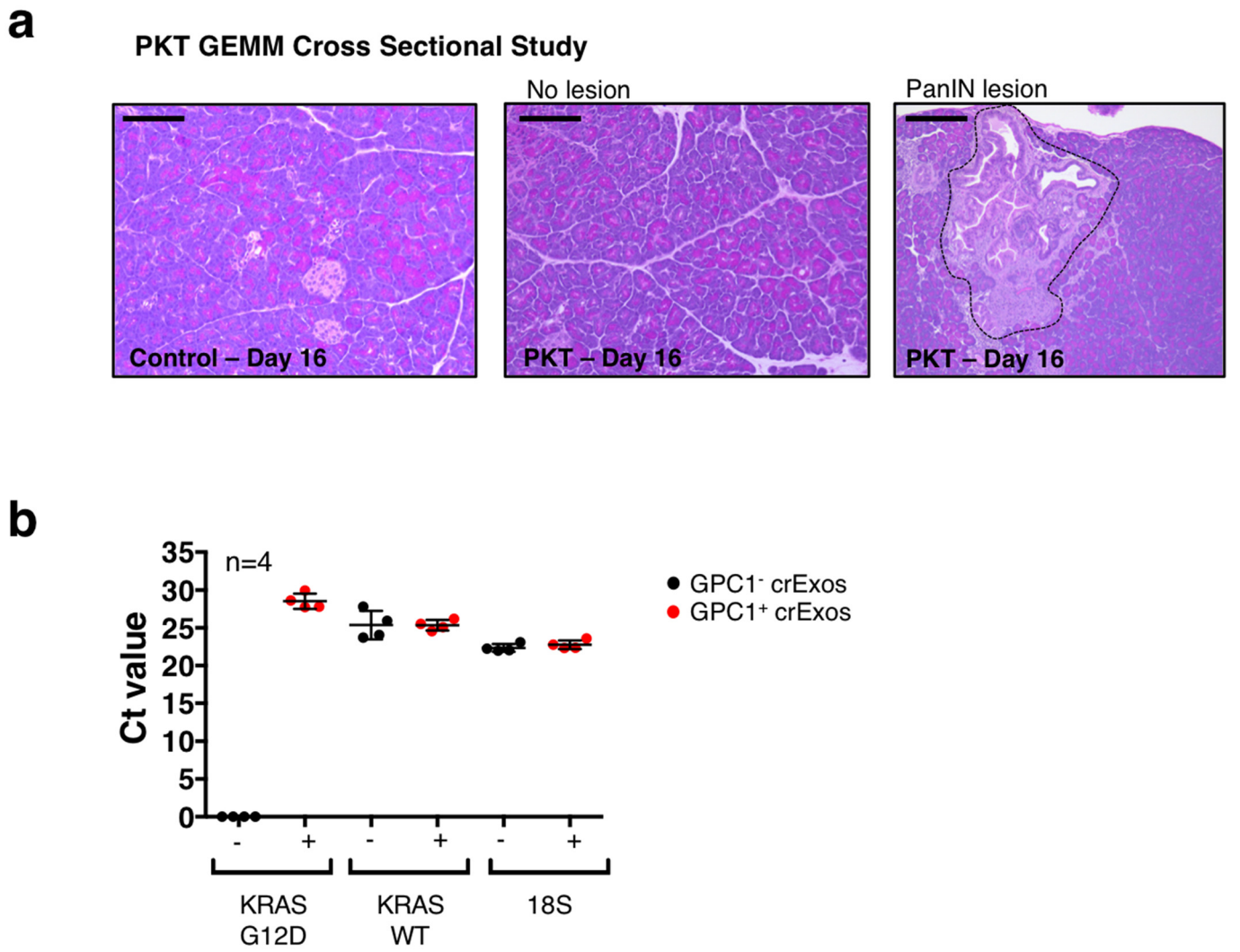

Extended Data Figure 7 | PDAC GEMM cross-sectional studies. **a**, Representative micrographs of haematoxylin-and-eosin-stained pancreas from 16-day-old control mice (left) and PKT mice presenting with (right, encircled) and without (middle) PanIN lesions. Scale bars, 100 μm. **b**, C_t values following qPCR analyses for oncogenic *KRAS*^{G12D}, wild-type *KRAS* and 18S internal control RNA from exosomes of 44–48-day-old PKT mice serum segregated using FACS for GPC1^{+}-bead-bound exosomes (red) and GPC1^{-}-bead-bound exosomes (blue). Data are mean ± s.d.

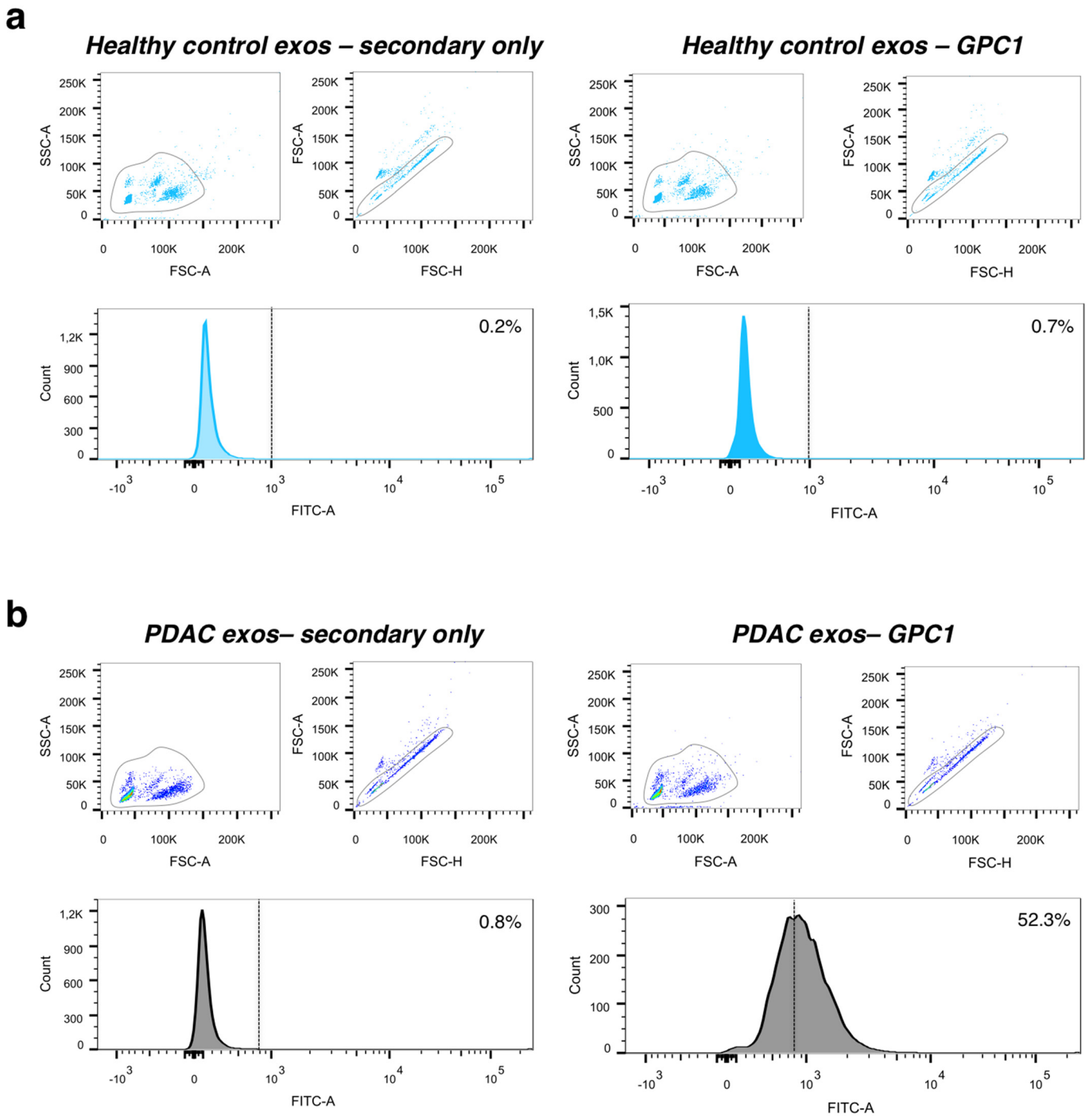

Extended Data Figure 8 | Raw scatter dot plot depicting flow cytometry analyses of beads with GPC1^{+}-bound exosomes **a**, Scatter plots and histogram of flow cytometry analyses of serum exosomes on beads of a representative healthy control (left panels are secondary antibody only; right panels are GPC1 antibody and secondary antibody). **b**, Scatter plots and histogram of flow cytometry analysis of serum exosomes on beads of a representative pancreatic cancer sample (left panels are secondary antibody only; right panels are with GPC1 antibody and secondary antibody).

Extended Data Table 1 | The 48 proteins exclusive to MDA-MB-231 exosomes and histopathological findings and scoring in PKT mice in the cross-sectional study

a

Protein Name	*Gene ID*	*Cellular Location*
ATP-binding cassette sub-family A member 6	ABCA6	Transmembrane
Tetraspanin-4	TSPAN4	Transmembrane
SLIT and NTRK-like protein 4	SLITRK4	Transmembrane
Putative protocadherin beta-18	PCDHB18	Transmembrane
Myeloid cell surface antigen CD33	CD33	Transmembrane
Glypican-1	GPC1	Membrane anchored

Protein Name	*Gene ID*	*Cellular Location*
Histone H2A type 2-A	HIST1H2AA	Nucleus
Histone H2A type 1-A	HIST1H1AA	Nucleus
Histone H3.3	H3F3A	Nucleus
Histone H3.1	HIST1H3A	Nucleus
Zinc finger protein 37 homolog	ZFP37	Nucleus
Hypermethylated in cancer 2 protein	HIC2	Nucleus
Zinc finger protein 12	ZSCAN12	Nucleus

Protein Name	*Gene ID*	*Cellular Location*
Laminin subunit beta-1	LAMB1	Secreted
Tubulointerstitial nephritis antigen-like	TINAGL1	Secreted
Peroxiredoxin-4	PRDX4	Secreted
Collagen alpha-2(IV) chain	COL4A2	Secreted
Putative protein C3P1	C3P1	Secreted
Collagen alpha-1(II) chain	COL2A1	Secreted
Hemicentin-1	HMCN1	Secreted

Protein Name	*Gene ID*	*Cellular Location*
Junction plakoglobin	JUP	Cytoplasm
Tubulin beta-2B chain	TUBB2B	Cytoplasm
Endoribonuclease Dicer	DICER1	Cytoplasm
E3 ubiquitin-protein ligase TRIM71	TRIM71	Cytoplasm
Katanin p60 ATPase-containing subunit A-like 2	KATNAL2	Cytoplasm
Protein S100-A6	S100A6	Cytoplasm
5'-nucleotidase domain-containing protein 3	NT5DC3	Cytoplasm
Valine--tRNA ligase	VARS	Cytoplasm
Kazrin	KAZN	Cytoplasm
ELAV-like protein 4	ELAVL4	Cytoplasm
RING finger protein 166	RNF166	Cytoplasm
FERM and PDZ domain-containing protein 1	FRMPD1	Cytoplasm
78 kDa glucose-regulated protein	HSPA5	Cytoplasm
Trafficking protein particle complex subunit 6A	TRAPPC6A	Cytoplasm
Squalene monooxygenase	SQLE	Cytoplasm
Tumor susceptibility gene 101 protein	TSG101	Cytoplasm
Vacuolar protein sorting 28 homolog	VPS28	Cytoplasm
Prostaglandin F2 receptor negative regulator	PTGFRN	Cytoplasm
Isobutyryl-CoA dehydrogenase, mitochondrial	ACAD8	Cytoplasm
26S protease regulatory subunit 6B	PSMC4	Cytoplasm
Elongation factor 1-gamma	EEF1G	Cytoplasm
Titin	TTN	Cytoplasm
Tyrosine-protein phosphatase type 13	PTPN13	Cytoplasm
Triosephosphate isomerase	TPI1	Cytoplasm
Carboxypeptidase E	CPE	Cytoplasm

Protein Name	*Gene ID*	*Cellular Location*
Putative rhophilin-2-like protein	RHPN2P1	Not specified
Ankyrin repeat domain-containing protein 62	ANKRD62	Not specified
Tripartite motif-containing protein 42	TRIM42	Not specified

b

Mouse ID	Age (days)	Sex	Genotype	GPC1 (%)	Normal (% area)	Involved (% area)	PanIN1a	PanIN1b	PanIN2	PanIN3	DCA	Other (defined)	Pathological score
T187	16	M	Healthy control	0.6	100	0	0	0	0	0	0		
T188	16	M	Healthy control	1.1	100	0	0	0	0	0	0		
T157	20	M	Healthy control	0.2	100	0	0	0	0	0	0		
T158	20	M	Healthy control	0.2	100	0	0	0	0	0	0		
T163	20	M	Healthy control	0.2	100	0	0	0	0	0	0		
T164	20	M	Healthy control	0.4	100	0	0	0	0	0	0		
T183	16	M	PKT	8.4	98.6	1.4	P	0	0	0	0		1
T190	16	F	PKT	5.2	100.0	0.0	0	0	0	0	0	reactive ducts	0
T191	16	F	PKT	6.4	100.0	0.0	0	0	0	0	0	reactive ducts	0
T156	20	M	PKT	8.3	100.0	0.0	0	0	0	0	0		0
T159	20	F	PKT	10.8	95.1	4.9	P	P	P	0	0		3
T160	20	F	PKT	9.8	99.3	0.7	P	P	0	0	0		2
T165	20	F	PKT	9.2	96.1	3.9	P	P	0	0	0		2

P : present
0 : not detected

a, Listing of the 48 proteins exclusively detected in exosomes from MDA-MB-231 cells determined by UPLC–MS and comparative analyses of exosomes derived from NIH/3T3, MCF 10A, HDF, E10 and MDA-MB-231 cells. The proteins are grouped based on cellular location. **b**, The mouse ID, age, genotype and percentage of $GPC1^+$ crExo beads of mice in the cross-sectional study are listed. A description of the histopathological findings and associated histological score is listed for PKT mice. Score 1: PanIN1a; score 2: PanIN1 a/b; score 3: PanIN2; score 4: PanIN3; score 5: ductal adenocarcinoma (DCA). P, present (lesions were detected). 0, no lesion detected.

Extended Data Table 2 | Demographics of patients and healthy participants and histological report of patients with chronic pancreatitis

a

	DISCOVERY COHORT No. of participants (n=321)	% of participants	VALIDATION COHORT No. of participants (n=82)	% of participants	No. of participants (n=32)	% of participants
	Pancreatic Cancer		Pancreatic Cancer		Breast cancer	
Total	190	59.19%	56	68.29%	32	100%
Sex						
Men	104	54.74%	28	50.00%	0	0%
Women	86	45.26%	28	50.00%	32	100%
Median Age (range)	66 (37 - 86)		70 (40 - 85)		57 (30 - 85)	
AJCC stage						
0	n.a.	-	n.a.	-	2	6%
I	2	1.05%	2	3.57%	12	38%
II	n.a.	-	n.a.	-	17	53%
IIa	19	10.00%	15	26.79%	n.a.	-
IIb	117	61.58%	36	64.29%	n.a.	-
III	11	5.79%	0	0.00%	1	3%
IV	41	21.58%	3	5.36%	n.a.	-
Tumor grade						
1	1	0.53%	1	1.79%	8	25%
2	91	47.89%	35	62.5%	13	41%
3	49	25.79%	19	33.93%	10	31%
4	1	0.53%	0	0.00%	n.a.	-
Unknown	48	25.26%	1	1.79%	1	3%
Tumor resected						
Yes	152	80.00%	54	96.43%	32	100%
No	38	20.00%	2	3.57%	0	0%
Neoadjuvant Radio-/Chemotherapy						
Received	10	5.26%	0	0.00%	0	0%
Not received	180	94.74%	56	100.00%	32	100%
	Benign Pancreatic disease (BPD)					
Total	26	8.15%				
Sex						
Men	18	69.23%	3			
Women	8	30.77%	3	50.00%		
				50.00%		
Median Age (range)	58.5 (31 - 77)		49 (43 - 56)			
Diagnosis						
Chronic pancreatits	15	57.69%	6	100%		
Autoimmune pancreatitis	3	11.54%	0	0.00%		
Serous cystadenoma	8	30.77%	0	0.00%		
	Pancreatic cancer precursor lesion (PCPL)					
Total	5	1.55%	0	0.00%		
Sex						
Men	2	40.00%	0	0.00%		
Women	3	60.00%	0	0.00%		
Median Age (range)	65 (59 - 74)		-	-	-	
Neoplasms						
IPMN	5	100.0%	0	0.00%		
	Healthy donors					
Total	100	31.15%	20	24.39%		

n.a. - non applicable

b

Patient No.	PanIN described	Histopathological report
1	No	Pancreatic tissue with chronic pancreatitis and extensive fibrosis and focal necrosis lipolytic and triptolytic areas.
2	No	Diffuse periductal lymphoplasmacytic infiltrates; severe periductal fibrosis and duct obstruction/disappearance; severe interlobular and acinar involvement; severe inflammatory storiform fibrosis and diffuse sclerosis; frequent venulitis and occasional arteritis; scattered and occasionally prominent lymphoid follicles
3	No	Chronic pancreatitis with periductal , inter- and intralobular fibrosis
4	No	Chronic pancreatitis and extensive fibrosis
5	No	Chronic recurrent and acute pancreatitis with plurifocal tryptolytic and lipolytic necrosis
6	No	Low-grade chronic pancreatitis with periductal fibrosis, in the present material no evidence of neoplastic events, no evidence of malignancy.
7	No	Chronic recurrent pancreatitis with some more pronounced fibrosis and intraductal calcifications. Chronic pancreatitis extends to the pancreas resection margin.
8	No	Chronic pancreatitis, cholangitis and papillitis with focally histomorphological aspect of an autoimmune, chronic sclerosing pancreatitis.
9	PanIN 1a	Pancreatic parenchyma (head of the pancreas) and peripancreatic fat and connective tissue with chronic recurrent pancreatitis with some areas fibrosis and abscesses. Pancreatic intraepithelial neoplasia (PanIN) Grade 1A.
10	No	Pancreatic parenchyma with perilobular fibrosis as well as dilated pancreatic ducts. In addition, peripancreatic fat and connective tissue with fibrosis. The finding represents a chronic pancreatitis.
11	PanIN 1a	Chronic-recurrent pancreatitis with pronounced fibrosis and dilated pancreatic ducts with focal inflammatory reactive epithelial cells. Older areas of organized necrosis and focal pancreatic intraepithelial neoplasia (PanIN) Grade 1A. Chronic pancreatitis also affects the pancreas resection margin.
12	No	Pancreatitis with focally accentuated, periductal, perilobular and intralobular fibrosis as well as smaller areas of organized fatty necrosis and presence of singel giant cells of foreign body type.
13	No	Chronic recurrent and acute pancreatitis with plurifocal tryptolytic and lipolytic necrosis with extensive destruction of the pancreatic parenchyma. Smaller secretion - and obliteration of pancreatic ducts with periductal fibrosis and localized squamous metaplasia. Peri- and interlobular fibrosis of the pancreatic parenchyma. Pancreatitis reaches the resection margin. At present, no neoplastic tissue, no evidence of malignancy.
14	No	Pancreatic tissue with some scarring chronic inflammation and chronic pancreatits. In the present material, no evidence of malignancy.
15	No	Tumor -free pancreatic tissue (surgical margins) with low periductal and interlobular fibrosis.

a, The group of IPMNs consist of 2 IPMN associated with a carcinoma *in situ*, 1 IPMN associated with an early adenocarcinoma of the pancreas (pT1), an IPMN with intermediate dysplasia and an IPMN with low-grade dysplasia. AJCC, American Joint Committee on Cancer. **b**, The histopathological report is listed for the 15 patients with chronic pancreatitis in the discovery cohort.